OPTIMIZATION OF SANDWICH-STYLE SERS SUBSTRATES FOR THE DETECTION OF HUMAN SKELETAL TISSUE COMPONENTS

A thesis presented to the faculty of the Graduate School of Western Carolina University in partial fulfillment of the requirements for the degree of Master of Science in Chemistry.

By

Kristin Kelly Cooke

Advisor: David D. Evanoff, Jr.
Associate Professor of Chemistry
Department of Chemistry & Physics

Committee Members: Brittania Bintz, Forensic Science Program
Dr. Kelly Grisedale, Forensic Science Program
Dr. Scott Huffman, Department of Chemistry & Physics

July 2016

ACKNOWLEDGMENTS

I would first like to thank my advisor, Dr. David Evanoff Jr., for his continued support and guidance with this research and throughout my time at WCU. He has helped me to discover the path to becoming the best version of myself, both as a student and emerging scientist, and for that I am incredibly grateful.

I would also like to thank Dr. Scott Huffman, Dr. Kelly Grisedale, and Brittania Bintz for serving on my thesis committee and for their invaluable encouragement and insightful comments regarding the direction and completion of this research.

I also gratefully acknowledge the Western Carolina Graduate School and the Chemistry and Physics Department for the grants, scholarships, and assistantships I have received that helped make this research possible.

Lastly, I must express my sincerest gratitude to my parents, Kelly Cooke and Sherry Rothrock, and to my boyfriend, Matthew Schiebel Jr., for providing me with unfailing support and continuous encouragement throughout my years of study and through the process of researching and writing this thesis. This accomplishment would not have been possible without them.

TABLE OF CONTENTS

LIST OF TABLES

LIST OF FIGURES

LIST OF ABBREVIATIONS

A	adenine
AEF	analytical enhancement factor
Ag ID	silver nanoparticle suspension
Ag_2O	silver (I) oxide
$AgNO_3$	silver nitrate
Ar^+	argon ion
C	cytosine
DNA	deoxyribonucleic acid
dNTP	deoxyribonucleotide triphosphate
FWHM	full width at half max
G	guanine
H_2O_2	hydrogen peroxide
H_2SO_4	sulfuric acid
HeNe	helium neon
LM	Lee-Meisel
mtDNA	mitochondrial DNA
NA	numerical aperture
Na_2SO_4	sodium sulfate
$NaNO_3$	sodium nitrate
OD	optical density
PCR	polymerase chain reaction
PVP	poly(4-vinylpyridine)
qPCR	quantitative polymerase chain reaction
SEM	scanning electron microscopy

SERS	surface enhanced Raman spectroscopy
SPPR	surface plasmon polaration resonance
STR	short tandem repeat
T	thymine

ABSTRACT

OPTIMIZATION OF SANDWICH-STYLE SERS SUBSTRATES FOR THE DETECTION OF HUMAN SKELETAL TISSUE COMPONENTS

Kristin Cooke

Western Carolina University (July 2016)

Advisor: Dr. David Evanoff, Jr.

Detection of DNA from various sources is an essential and delicate process that plays a key role in the analysis of biological evidence. As such, the extraction of DNA from bone is a widely studied area in forensic science. Unfortunately, there is no standard pre-extraction technique to qualitatively assess the likelihood of obtaining a usable amount of high quality DNA for genotyping. The purpose of this research is to lay the foundation for investigating Raman spectroscopy and surface enhanced Raman spectroscopy (SERS) as potential diagnostic tools for determining whether a bone sample contains viable DNA for genotyping. Herein, we present individual spectra of skeletal tissue and DNA components measured using both Raman spectroscopy and SERS. A previously studied fabrication method for a SERS substrate architecture, known as sandwich-style SERS substrates, was utilized for this research. A key focus of this research was to optimize these substrates to enable to detection of low concentrations of adenine, which serves as a Raman-active marker molecule for the detection of DNA in various solutions. Several parameters were varied from the original substrate fabrication method such as silver nanoparticle size, dispersion, and inter-particle spacing - the result of which yielded SERS substrates that led to the detection of adenine molecules in a solution with a concentration as low as 10^{-8} M.

CHAPTER 1: BACKGROUND

DNA collection is a vital process that plays a pivotal role in everything from crime scene investigation to diagnostic screening in clinical medicine.[1,2] In many forensic cases, calcified tissues are sometimes the only accessible source of DNA. Since a standard screening method has not been established to qualitatively assess the likelihood of obtaining amplifiable, high quality DNA from skeletal tissue, it is often a severe setback when the sample fails to be genotyped due to degradation or lack of DNA. For example, it typically takes several days and many expensive laboratory supplies and reagents to extract, quantify, and genotype a single bone sample. One alternative is the use of Raman spectroscopy or surface enhanced Raman spectroscopy (SERS) to detect DNA. This screening tool could be used as a confirmatory test to assess DNA viability prior to quantification and genotyping, or perhaps even before extraction from a bone sample. While this research does not provide a means by which to detect degraded or non-degraded DNA in a bone sample, it is in the scope of this project to lay the groundwork for such an application by using substrates that have been optimized for the detection of skeletal tissue and DNA components.

1.1 Human Bone Composition & Quality Analysis

Bone is a composite material that consists of a mineral and matrix component, and for each individual bone there is a unique mineral to matrix ratio that is indicative of bone quality.[3] Bone is categorized as either trabecular bone - the inner, "spongy" bone - or cortical bone, which is the hard, outer covering of bone. Both classes of bone are made up of bone tissue which consists of two main components: approximately 65% mineral and 35% matrix by mass; these percentages vary slightly based on the type of bone being analyzed.[4] The mineral phase contains calcium hydroxyapatite crystals and the organic phase is primarily type I collagen, which is a triple-helical molecule that consists of chain-like fibrils.[5] Cortical

bone is relatively dense because of its many microscopic channels and forms the outer wall of all bones and the diaphysis, or shaft, of long bones. It is largely responsible for the supportive and protective function of the skeleton. Almost 80% of the mass of the adult human skeleton is cortical bone, while the remaining 20% is trabecular bone.[4] Bones are also often a source of intact DNA and the recovery of genetic material from preserved hard skeletal remains is an essential part of ancient DNA, archaeological and forensic research. However, there is little understanding about the relative concentrations of DNA within different skeletal tissues, the impact of sampling methods on DNA yields, or the role of environmentally-determined degradation rates on DNA survival in specimens.[6,7]

As we age there are many changes that bones undergo due to loss of bone mass, changing bone mineralization, and changes in fracture toughness of bones.[4,8] These changes in bone can be observed not only qualitatively, but quantitatively as well using different mechanical tests, such as tensile and compression tests, Fourier transform infrared imaging, and Raman spectroscopy.[3,4,9] Since using Raman spectroscopy is a central technique used in this research, it is important to note previous assessments of skeletal tissue for forensic applications using Raman and SERS. Using Raman spectroscopy, a mineral to matrix ratio can be calculated for an individual bone by identifying the unique changes in band area that correspond to phosphate (mineral) and amide (matrix) bands. The changes in these spectral bands correspond to information about bone mineralization, bone fragility, and chemical or radiological insults to bone.[3,10–14] This concept of gaining quantitative and qualitative information about changes due to different materials in skeletal tissue using Raman spectroscopy is a central idea of the long term goals of this research.

1.2 DNA Structure and Common Analysis Techniques

Deoxyribonucleic acid (DNA) is the complex molecule that carries genetic instructions used in the development and reproduction of all known living organisms. A majority of DNA

is located in the cell nucleus, where it is called nuclear DNA, but a small amount of DNA can also be found in the mitochondria, where it is called mitochondrial DNA (mtDNA). The information in both types of DNA is stored as a code using different combinations of four bases: adenine (A), guanine (G), cytosine (C), and thymine (T). Adenine and guanine are double-ringed larger molecules, called purines, and cytosine and thymine are single-ringed smaller molecules, called pyrimidines. The human genome consists of about 3 billion bases, and more than 99% of the sequence of those bases are the same in all people.[15] Each base is covalently bonded to a deoxyribose sugar molecule and at least one phosphate molecule. Together, a base, sugar, and phosphate are called a nucleotide, or deoxyribonucleoside triphosphate (dNTP). When dNTPs link together, the $3'$ carbon of one sugar molecule is connected through a phosphate group to the $5'$ carbon of the next sugar, and the resulting structure is a single strand of DNA. This linkage is also called a $3'$-$5'$ phosphodiester linkage, and forms the negatively charged backbone of all DNA strands. In double-stranded DNA, the bases pair up through hydrogen bonds such that A pairs with T and G pairs with C. Since the A-T base-pair only has two hydrogen bonds and the G-C base-pair has three hydrogen bonds, the G-C regions of DNA are stronger and the A-T regions are more susceptible to thermal fluctuations and breakage. A section of double-stranded DNA including an example of each type of base-pair and the sugar-phosphate backbone is shown below in Figure 1.

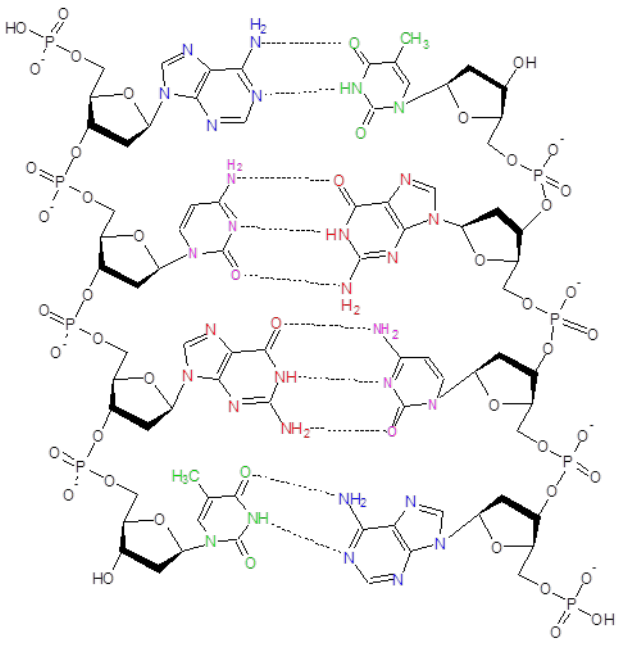

Figure 1. An example of the different base-pairs that undergo hydrogen bonding to make up a section of double stranded DNA, where adenine (blue) interacts with thymine (green), and guanine (red) interacts with cytosine (pink).The negatively charged phosphate molecules linked together by deoxyribose form the outside of the structure and the backbone of DNA.

Analysis of DNA from various matrices such as bone, hair, and bodily fluids is an essential process that is key in many areas of forensic and clinical sciences. In order to be analyzed, first the DNA must be extracted from a sample. There are many techniques that are commonly used to extract DNA from different sample types including phenol-chloroform purification and magnetic bead-based extraction.[16] Once DNA has been extracted, the amount of extracted DNA can be determined using rapid spectrophotometric or fluorimetric methods, or the slower, more accurate and sensitive quantitative PCR (qPCR). The latter method of DNA quantification utilizes the polymerase chain reaction (PCR) in which certain parts of the genome are exponentially copied. Two common methods for the detection of PCR products in qPCR are nonspecific fluorescent dyes that intercalate with any double stranded DNA, and sequence specific DNA probes. All of these methods (spectrophotometry, fluorimetry and qPCR) also yield information regarding the quality of the DNA that has been

extracted to a certain degree.[17] After the DNA is quantified and an initial assessment of quality has been made, the correct amount of DNA can be amplified by PCR during which highly polymorphic regions of DNA, known as short tandem repeats (STRs), are exponentially copied and analyzed using capillary electrophoresis.

1.3 DNA Detection in Bones

In some forensic cases skeletal tissue may be the only accessible source of DNA. After extraction, DNA from the bone sample is quantified, then amplified and genotyped, as previously discussed. The resulting data is then compared to reference data to determine a contributor. Current DNA genotyping methods involve the use of extremely costly equipment and reagents, and the workflow is labor intensive and often takes several days to yield interpretable data. Since a standard screening method has not been established for determining whether DNA in bone is of requisite quality for genotyping prior to extraction, it is often severely disadvantageous for the aforementioned reasons when the sample fails to be genotyped due to degradation or lack of DNA.

1.4 Raman Spectroscopy and SERS

1.4.1 Introduction to Raman Spectroscopy

In Raman spectroscopy, monochromatic light from a laser or other source is used to investigate the vibrational modes in a system. Molecules in the ground state are bombarded with laser light and a portion of the molecules move to a theoretical "virtual energy state". After the photon interacts with the molecule, the photon is scattered with the same, more, or less energy than before the interaction with the molecule.

When the energy of an incident photon is unaltered after collision with a molecule, the photon's frequency remains the same upon scattering; this elastic scattering event is the most common and is called Rayleigh scattering. In the Raman Effect, however, incident

light is inelastically scattered from a sample (energy is transfered between the molecule and the photon) thus shifting in frequency by values equivalent to particular vibrational modes within the analyte molecule. Inelastic scattering results in a photon that is either lower in energy (Stokes shift) or higher in energy (anti-Stokes shift) than the incident photon, as seen in the Jablonski diagram in Figure 2. The energy difference in the photon corresponds to the energy gap between the ground vibrational state and the first excited vibrational state.

The Raman spectrum is a plot of scattered intensity as a function of the change in frequency before and after the scattering event. The loss or gain in photon energies corresponds to the difference in final and initial vibrational energy levels of the molecules participating in the interaction. The resultant spectra are characterized by shifts in wavenumbers from the incident frequency. Raman spectroscopy has many advantages over other spectroscopic techniques since the Raman Effect can be observed under ambient conditions with minimal sample preparation required. New advances in optical fiber probes have also facilitated sample measurement by bringing excited light to a sample that may be difficult to move and enables remote detection of Raman signals.[18]

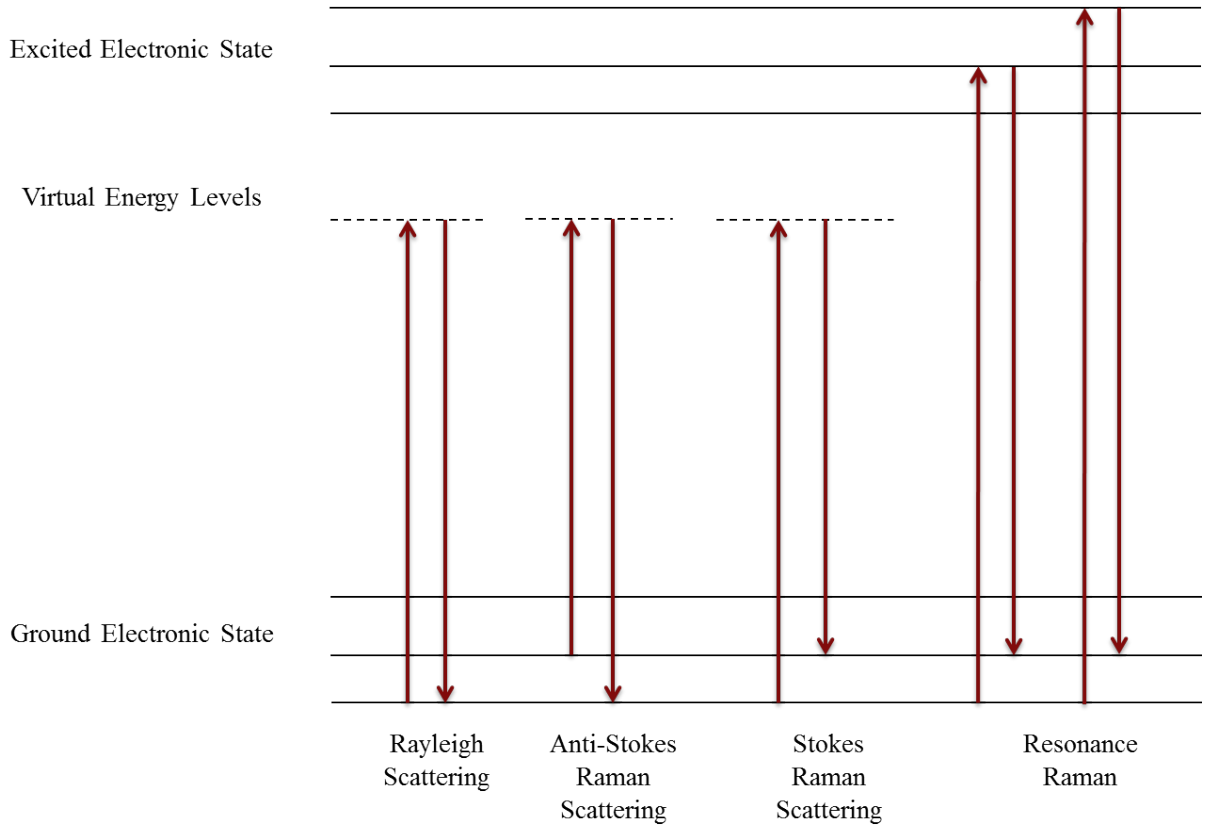

Figure 2. Jablonski diagram of Rayleigh scattering and different types of Raman Scattering.

1.4.2 Enhancement of the Raman Effect

The main disadvantage of the Raman effect is that Raman scattering is observed significantly less frequently than Rayleigh scattering; about one in ten million photons that are scattered result in an inelastic scattered photon.[19] For that reason, methods of enhancement are typically used to improve the amount of Raman scattering that occurs. Resonance Raman is one such method that utilizes laser light of the same frequency as the energy needed to excite an appropriate electronic transition in a material.[20] Another method that is becoming more popular is surface enhanced Raman spectroscopy (SERS). In early experiments that involved measuring pyridine on electrochemically roughened silver electrodes, a

large increase in Raman signal was observed.[21] The signal increase was determined not to be due to an increased number of molecules adsorbed to the surface, but instead was directly linked to how the substrate was prepared. The so called "SERS-active substrates" employ various metal structures or particles with a range of sizes.[20] The most common types of SERS active substrates are roughened silver or gold electrodes and aggregates of silver or gold nanoparticles in the 10 nm to 150 nm size range.[20] Recent advances have led to many biological applications of SERS, such as the ability to detect biological warfare agents, medical diagnostics for cancer, diabetes, and other diseases, and detection of DNA in very low quantities, which is one of the potential applications of this research.[10,22–25] In contrast to IR spectroscopy, the Raman signal of water molecules is very small, allowing DNA and other biological samples to be observed in their native aqueous environment while still being easily distinguishable from the background.

When electromagnetic radiation strikes the surface of the metal substrate, collective oscillations of the conduction electrons are excited and are known as surface plasmon polaration resonances (SPPRs).[26] When SPPRs are excited in a single metal particle, the oscillating electrons generate an electromagnetic field that propagates away from the surface of the particle. Enhancement by SERS substrates occurs when the electric field produced from the silver that propagates away from the metal surface overlaps with an analyte molecule which then experiences an increased induced polarization. The enhancement of a Raman cross section by SPPRs is greatest when the direction and frequency of this propagating electric field is in resonance with the direction and frequency of the polarization of an analyte molecule, yielding enhancement factors as high as fourteen orders of magnitude higher than that of a normal Raman measurement.[27]

1.4.3 Sandwich SERS-Active Substrates (synthesis)

As discussed previously, the most common types of SERS active substrates are roughened silver or gold electrodes and aggregated nanoparticle suspensions.[20] One type of SERS active substrate that combines metal films and silver nanoparticle arrays to form easily controlled "roughened electrodes" is the nanoparticle mirror sandwich SERS substrate. These substrates exploit the plasmon coupling between a single layer of silver nanoparticles and a smooth, continuous silver film with analyte molecules sandwiched in between to provide enhancement.[28] The substrates are assembled first by coating a small glass microscope slide with poly(4-vinylpyridine) (PVP) to facilitate adhesion of the smooth silver film. Next a smooth silver film is deposited on the substrate using electrothermal evaporation of silver under high vacuum conditions. Another layer of PVP is added, and then the substrates are exposed to a nanoparticle suspension for several days to assemble a two-dimensional array of the particles. A schematic diagram of the completed sandwich SERS substrates is shown in Figure 3.

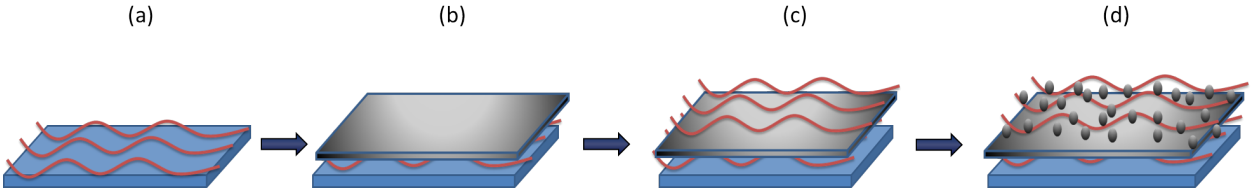

Figure 3. Schematic diagram of the synthesis of a sandwich SERS substrate showing (a) the first layer of PVP on a cleaned glass slide, (b) a smooth silver film layer, (c) the second layer of PVP, and lastly (d) a layer of silver nanoparticles

There are several well-studied methods for synthesizing silver nanoparticle suspensions that can serve as the outer layer for these substrates. The Lee-Meisel (LM) method, also known as a trisodium citrate reduction, involves the reduction of silver nitrate ($AgNO_3$) with trisodium citrate.[29] The resulting silver particles are coated with citrate and are poly-

dispersed in size. The citrate coating on the particles in suspension is advantageous because it helps to protect the particles from aggregation. The second method of silver particle synthesis, known as the hydrogen reduction method, utilizes hydrogen gas to reduce silver (I) oxide (Ag_2O).[30] The particles grow slowly over the course of a few hours which results in a monodispersed suspension of low-aspect ratio silver particles. The diameter of the hydrogen reduced silver particles is easily monitored and is proportional to the time that the reaction is allowed to proceed, thus making this method extremely useful when size of the resulting particles is relevant.[30] One drawback to this method though is that the reaction produces up to 10% high-aspect ratio particles (rods) as a byproduct. As a result, if a more monodispersed suspension is desired, the particle suspension must be filtered to lower the concentration of the rods so that the suspension is more uniform and the overall plasmon resonance of the suspension is not affected.

One advantage to using these sandwich style substrates is that coupling between particles can also be utilized in addition to the particle-film coupling.[31] In addition to the single particle plasmons that were previously discussed, collective plasmons of two or more close particles can be observed. Coupling is the result of the interaction of the local electromagnetic fields that extend away from the surface of the particles undergoing an SPPR. In order for coupling to occur, the particles must be close enough so that the electromagnetic fields can interact with each other, which can be achieved by assembling silver particles in 1D or 2D arrays.[31–33] When the distance between the particles in the array is similar to that of the collective SPPR wavelength, constructive interference occurs between the electromagnetic field near the particles in the array and the resulting electric field between the particles becomes much stronger.[34,35]

CHAPTER 2: INTRODUCTION TO RESEARCH

The purpose of this research is to develop methods for Raman spectroscopy and surface enhanced Raman spectroscopy (SERS) screening of skeletal tissue and DNA components. Ultimately, this spectroscopic technique will be explored for use as a diagnostic tool to determine whether a bone sample contains amplifiable DNA prior to extraction and genotyping. Previous research has shown that the nucleotides that comprise DNA can be detected using SERS, and that Raman spectroscopy has been used to evaluate changes in bone composition.[3,10–14] With this background knowledge of how to collect Raman spectra of DNA and bone components, the purpose of this research is to report characteristic spectra of different skeletal tissue and DNA components and to investigate the synthesis and optimization of different sandwich style SERS substrates for measuring low concentrations of DNA components.

The first goal of this research was to present individual Raman spectra of skeletal tissue and DNA component powders using no SERS enhancement. Spectra of calcium hydroxyapatite powder, powdered human femur bone, DNA base powders, and solid 2-deoxy-D-ribose were all collected using measurement parameters optimized for these samples.

The second goal of this research was to develop a method to fabricate sandwich SERS substrates that is optimized for measuring solutions containing the components of DNA. Sandwich SERS substrates utilize a smooth silver film and silver nanoparticles in close proximity to analyte molecules to provide enhancement by particle-film interactions (coupling). This research investigates the notion that both particle-film coupling and inter-particle coupling have a positive impact on the enhancement of Raman signal. To manipulate the enhancement by such interactions, several fabrication parameters were varied such as the silver nanoparticle synthesis method, the particle size, the particle concentration, and the inter-particle spacing.

The third goal was to utilize Raman spectroscopy and SERS to obtain spectra of a Raman-active molecule, adenine, present in DNA base and nucleotide solutions. The optimized sandwich SERS substrates previously mentioned were used to detect low concentrations of adenine in solution to determine the degree of enhancement that the substrates yield when compared to plain Raman spectroscopy measurements.

Future projects can also be proposed from the data that was collected in this study. Controlled studies will be performed using the aforementioned substrates to further investigate the factors that influence the enhancement of relevant DNA samples. Having a substrate that is optimized to detect the presence of adenine, and by extension DNA, will allow for further studies to investigate the likelihood of detecting DNA from various sources.

CHAPTER 3: EXPERIMENTAL

3.1 Materials

2-deoxy-D-ribose (99%), and cytosine powder (99+%) were purchased from Acros Organics. Purified human collagen (type I) was purchased from Advance BioMatrix. Guanine powder (98%) and poly(4-vinylpyridine) (PVP, MW = 60,000) were purchased from Aldrich Chemical Company. Compressed nitrogen gas and liquid nitrogen were received from Andy Oxy Company and hydrogen gas (research grade, 99.9999%) was received from National Specialty Gases. Fisherbrand type 1 vials and plain glass microscope slides were used for all sandwich SERS substrates. Silver nitrate ($AgNO_3$, 99.9%), sodium nitrate ($NaNO_3$, 99%), sulfuric acid (H_2SO_4, 95%), sodium sulfate (Na_2SO_4, 99.5%), 90 mm nylon supported membrane 0.45 µm and 0.22 µm filters, hydrogen peroxide (H_2O_2, 30%), trisodium citrate dihydrate (99.6%), calcium phosphate tribasic, and silver (I) oxide (Ag_2O, 99.99%) were all purchased from Fischer Scientific. Silver pellets (99.99%) were purchased from Kurt J. Lesker. Ethyl alcohol (ACS Grade, 200 proof) was received from Pharmco-Aaper. Ultrapure dNTPs (100 mM) and control DNA (10 ng/µL) were obtained from Promega. Adenine and thymine powders (99%) were purchased from Sigma. DNA suspension buffer (10 mM Tris-HCl, 0.1 mM EDTA pH 8.0) was purchased from Teknova. All human skeletal remains were purchased from Skulls Unlimited. Water with nominal resistivity of 18 MΩ · cm was obtained from a Barnstead NANOpure Diamond system with a 0.2 µm hollow fiber filter. All chemicals were used as purchased with no further purification.

3.2 Instrumentation & Equipment

Particle suspensions were analyzed in an open atmosphere Agilent 8453 UV-Vis system. All Raman spectra were measured on a Horiba Jobin Yvon LabRamHR Raman microscope using

a 10x or 100x objective with numerical apertures (NAs) of 0.25, and 0.90, respectively. The excitation lasers included the 632.8 nm line from a helium neon (HeNe) laser (Horiba Jobin Yvon, Edison, NJ), and varying powers of the 514.1 nm and 457.9 nm lines from an argon ion (Ar^+) laser (Spectra-Physics, Santa Clara, Ca). Also, all spectra were measured with either a 600 groove/mm grating or an 1800 groove/mm grating, and a TE-cooled CCD detector. The Raman software used was HORIBA Scientific LabSpec 6, which contained a mapping and auto focus feature that was useful in reducing human error when focusing across various sample substrates. All glassware and microscope slides were plasma cleaned before use with a Harrick Plasma PDC-32 plasma cleaner. All silver films were deposited using a Denton Vacuum DV-502A deposition system. A Hitachi S-4800 scanning electron microscope (SEM) operating at 12 kV and 15 µA was employed to image all SERS substrates.

3.3 Ag Particle Synthesis

3.3.1 Lee-Meisel Nanoparticles

A suspension of Lee-Meisel (LM) particles was prepared for SERS studies. Silver nitrate (90 mg) was dissolved in approximately 500 mL of NANOpure water and brought to boiling. A solution of 1% sodium citrate (10 mL) was added and the solution was kept boiling for approximately one hour. The resulting sols were brownish-green in color and were determined by SEM to be polydispersed, with an optical density (OD) of 13.6 and an average dipole maximum at 406 nm. The suspension was then allowed to cool under gentle stirring and stored in a plasma cleaned glass container. The extinction spectrum and associated SEM image of the LM particles used for the sandwich SERS substrates in the following experiments are shown in Figure 10.

3.3.2 Hydrogen Reduction Nanoparticles

Several different-sized particle suspensions prepared by hydrogen reduction of Ag_2O made previously by this lab were obtained. An aqueous solution of saturated Ag_2O was reduced with hydrogen gas in a large three-neck reaction vessel. The vessel was filled with 3 L of NANOpure water and 3 g of Ag_2O was added. The solution was heated to 70 °C and pressurized to 10 psi above atmosphere with hydrogen gas. The suspensions were successively filtered with 0.45 µm and 0.22 µm nylon filters. The particle suspensions were then centrifuged at 150 times gravity for 8 hours at 4 °C to concentrate the particles for later use. A total of three different sizes of silver nanoparticles were used in these experiments with dipole maxima of 430 nm (OD 19.5), 491 nm (OD 161.3), and 582 nm (OD 286.3) for particle suspensions A, B, and C, respectively.

3.4 Measuring Ag Particle Coupling in Sandwich SERS Substrates

To observe silver particle coupling, a previously published method was followed.[31] Plasma cleaned glass microscope slides were first immersed in a 2% (w/w) PVP/ethanol solution and were left to slowly spin vertically on a Barnestead Thermolyne Labquake® rotisserie style vial holder for several hours. Then, following thorough rinsing with ethanol and water, the slides were dried under a stream of compressed nitrogen. The slides were then annealed in an oven at 100 °C for one hour and were immersed in the aforementioned silver particle suspensions prepared using hydrogen reduction where they were left to slowly spin vertically on the rotisserie for at least two days. The slides were then rinsed and coupling was assessed using ultraviolet-visible spectroscopy (UV-Vis) to observe the band shape of the resulting dipole. In order to obtain different degrees of coupling, several parameters were varied from the original synthesis including slide cleaning method by plasma cleaning or by rinsing with a 1:3 mixture of 30% H_2O_2/H_2SO_4 (piranha solution), weight percent of PVP solution,

annealing time, annealing temperature, the addition of Na_2SO_4 salt, suspension type, particle concentration, and slide orientation exposed to the silver particles. To achieve different slide orientations during coating, the vials that contained the slides in silver particle suspension were attached to the rotisserie either vertically or horizontally, as shown in Figure 4.

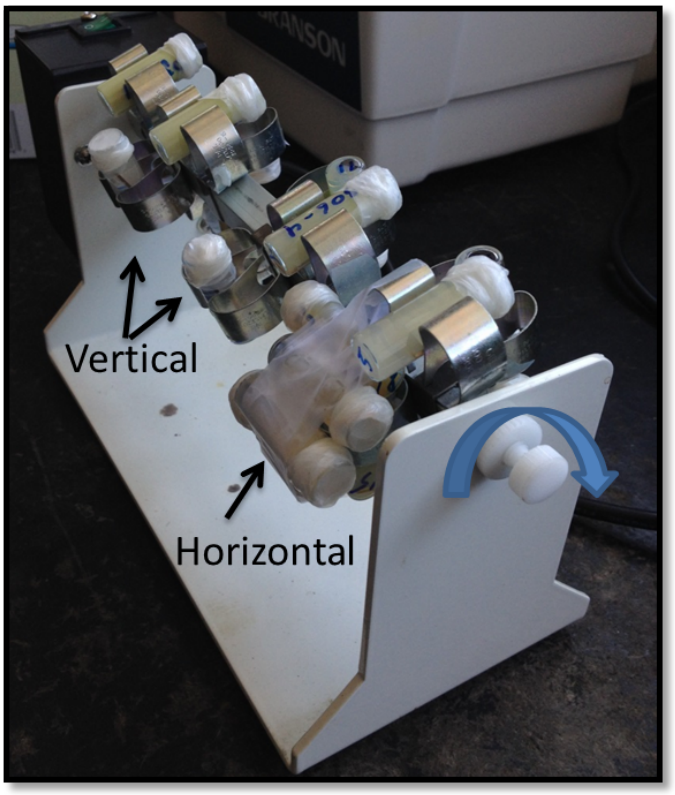

Figure 4. The horizontal and vertical orientations of vials containing a substrate and silver particle suspensions affixed to a rotisserie.

3.5 Fabrication of Smooth Ag Mirror Films

To synthesize SERS substrates, a previously published method was followed.[28] Plasma cleaned glass microscope slides were first immersed in a 2% (w/w) PVP/ethanol solution and were left to slowly spin vertically on a Barnestead Thermolyne Labquake® rotisserie style vial holder for several hours. Then, following thorough rinsing with ethanol and water, the slides were dried under a stream of compressed nitrogen. The slides were then annealed

in an oven at 100 °C for one hour and were placed directly into the evaporation chamber of a Denton vacuum evaporator. The chamber was pumped down over the period of an hour using an oil diffusion pump to achieve an ultimate vacuum pressure of 2.0×10^{-6} Torr. A current was then applied across two electrodes connected by a wire basket that held a solid silver pellet. Silver was deposited on the PVP coated microscope slides with a deposition rate ranging between 2.0 Å/s to 2.8 Å/s for approximately 10 minutes and yielded a layer of silver that was approximately 100 nm thick. As the metal was deposited, the appearance of the films changed from clear to a slightly blue tint and finally a shiny mirror-like surface. The film consists of a continuous layer of silver islands at an average film thickness of 10 nm. At 50 nm the substrate appears mirrored due to the film thickness increasing past the skin depth of silver metal.[28]

3.6 Fabrication & Characterization of Mirror Sandwich SERS Substrates

The silver mirror films were further modified with another layer of 2% PVP functioning as a coupling layer for the silver nanoparticles. The silver films were immersed once again in a 2% (w/w) PVP/ethanol solution and were left to slowly spin vertically on the same rotisserie style vial holder for several more hours. Then, following thorough rinsing with ethanol and water, the slides were dried under a stream of compressed nitrogen. The slides were then annealed in an oven at 100 °C for one hour and were immersed in the aforementioned silver particle suspensions where they were left to slowly spin vertically on the rotisserie for at least two days to allow the particles to saturate the surface of the film. The slides were then rinsed and stored in NANOpure water for later use.

3.7 Raman/SERS Measurements

3.7.1 Measurement Specifications

A silicon standard reference material was used before each set of measurements to properly align the laser spot as well as to account for any differences in spectra between Raman spectrometers, instrumental setup, sample preparation and other factors that affect Raman spectra. The power of the laser line at the the laser source as well as at the sample were measured daily before any Raman or SERS measurements were collected. Using the 10x microscope objective, the substrate (plain glass slide or sandwich SERS substrate) was brought into focus, then defocused +450 µm in the z axis to account for the difference in focal lengths between the visual CMOS camera and spectral CCD camera. A background spectrum of each SERS substrate was collected that was representative of all positions across the substrate. Then the microscope was defocused another +25 µm to +50 µm in the z axis for any solution samples so that the measurement was collected right above the substrate while still in solution. Unless otherwise noted, all background and sample spectra were collected using an 1800 groove/mm grating and 1 s acquisition for 3 accumulations.

3.7.2 Bone Preparation

Bone samples were obtained from the Forensic Science Program at Western Carolina University. Femur bone cross sections were taken using a sterilized bone saw, while cortical outer bone samples were excised using a Dremel rotary tool, and excess bone powder was also collected that was generated by the Dremel rotary tool. Safety and cleaning procedures for preventing DNA contamination were used when collecting all bone samples. A lab coat and gloves were worn to protect against any direct contamination. All of the tools, glassware, and surfaces used were either autoclaved, bleached, or UV cleaned. Also, a new, sterilized, disposable Dremel rotary tool bit was used for each excision.

3.7.3 DNA Base Preparation & DNA Component Analysis

DNA base powders (adenine, guanine, cytosine, and thymine) and solid 2-deoxy-D-ribose were measured using the 632.8 nm HeNe laser line and a 100x microscope objective using Raman on plain glass slides. Adenine powder (0.50 g) was dissolved in NANOpure water and was sonicated to form a 0.15 M stock base solution. A series of dilutions were made in order establish the limit of detection of adenine using different sandwich SERS substrates. Concentrated solutions of the other bases could not be prepared due to solubility issues with solvents compatible with SERS substrates. To measure the adenine solutions, dNTP solutions, and DNA suspension buffer, 10 µL of each were placed on different positions of a single sandwich SERS substrate (shown in Figure 5) and spectra were collected using the 632.8 nm HeNe laser line and 10x microscope objective.

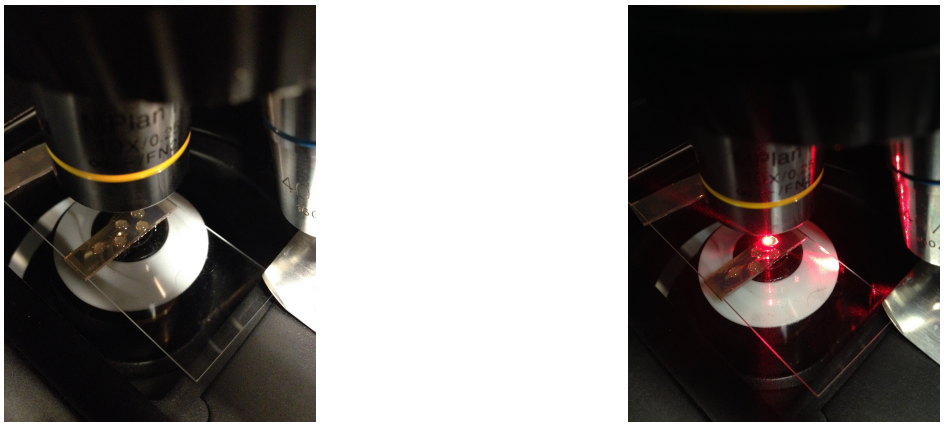

(a) (b)

Figure 5. (a) 10 µL of DNA base solution under a 10x microscope objective on a single sandwich SERS substrate and (b) the same substrate and solution with the 632.8 nm HeNe laser on during spectrum collection.

CHAPTER 4: RESULTS & DISCUSSION

4.1 Analysis of Human Skeletal Tissue and Bone Components

The components that make up bone are much more abundant than DNA in these calcified tissues. This means that it is important to be able to obtain spectra under similar collection conditions (e.g. laser frequency, grating, microscope objective, etc.) of the skeletal tissue as well as individual components of bone in order to eventually distinguish between Raman bands that originate from bone components and DNA.

4.1.1 Raman Spectroscopy of Human Bone Powder

A reference spectrum of a mouse tibia was first obtained from the literature and used as an initial reference for assigning correct band position and relative intensity compared to other bands.[3] The literature spectrum also served as a breakdown of what compounds in the bone correspond to each chemical shift.[3] The spectrum of the mouse tibia was then compared to several spectra collected from a human femur bone; the bands indicative of calcium phosphate (mineral) and collagen (matrix) groups in both the literature and measured bone spectra were in identical positions, so it can be concluded that the mouse bone reference spectrum is comparable to bones from human sources. The bands that correspond to the mineral components of bone are approximately $425\,\mathrm{cm}^{-1}$, $598\,\mathrm{cm}^{-1}$, $960\,\mathrm{cm}^{-1}$, and $1060\,\mathrm{cm}^{-1}$, and $1270\,\mathrm{cm}^{-1}$, $1450\,\mathrm{cm}^{-1}$, and $1690\,\mathrm{cm}^{-1}$ for the matrix components; these bands are identified in Figure 6.

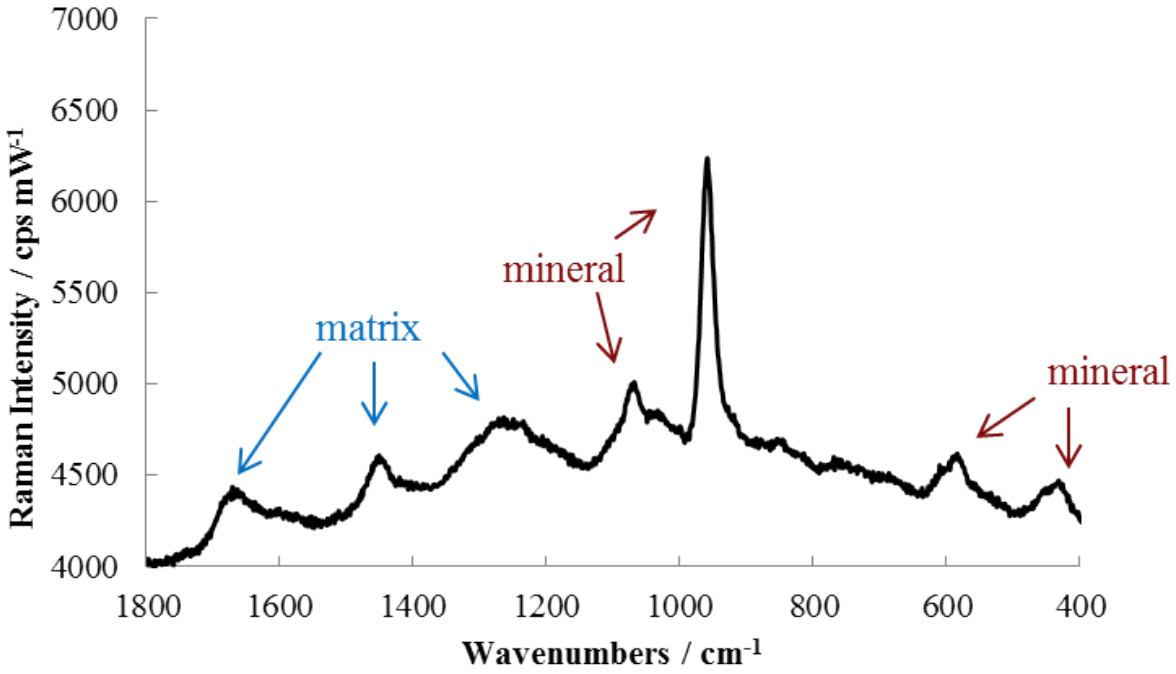

Figure 6. Raman spectrum of plain femur bone powder with mineral and matrix bands labeled.

Several types of bone, including cortical, trabecular, and a powdered mixture of both, were measured in order to determine if different matrices influence band position, but there were no observable shifts detected in the Raman spectra. Raman spectra of calcium phosphate tribasic powder and lyophilized type I human collagen, which are the individual components that skeletal tissue consists of, were then measured using Raman. The spectrum for calcium phosphate, which constitutes the mineral component of bone, is shown in Figure 7. As expected, compared to the spectrum of bone powder, only mineral-specific Raman bands are observed in the spectrum of calcium phosphate tribasic. The spectrum of collagen was much more difficult to collect since it produced highly fluorescent spectra even after several parameters were changed (such as varying exposure time and using a solid form of collagen instead of liquid).

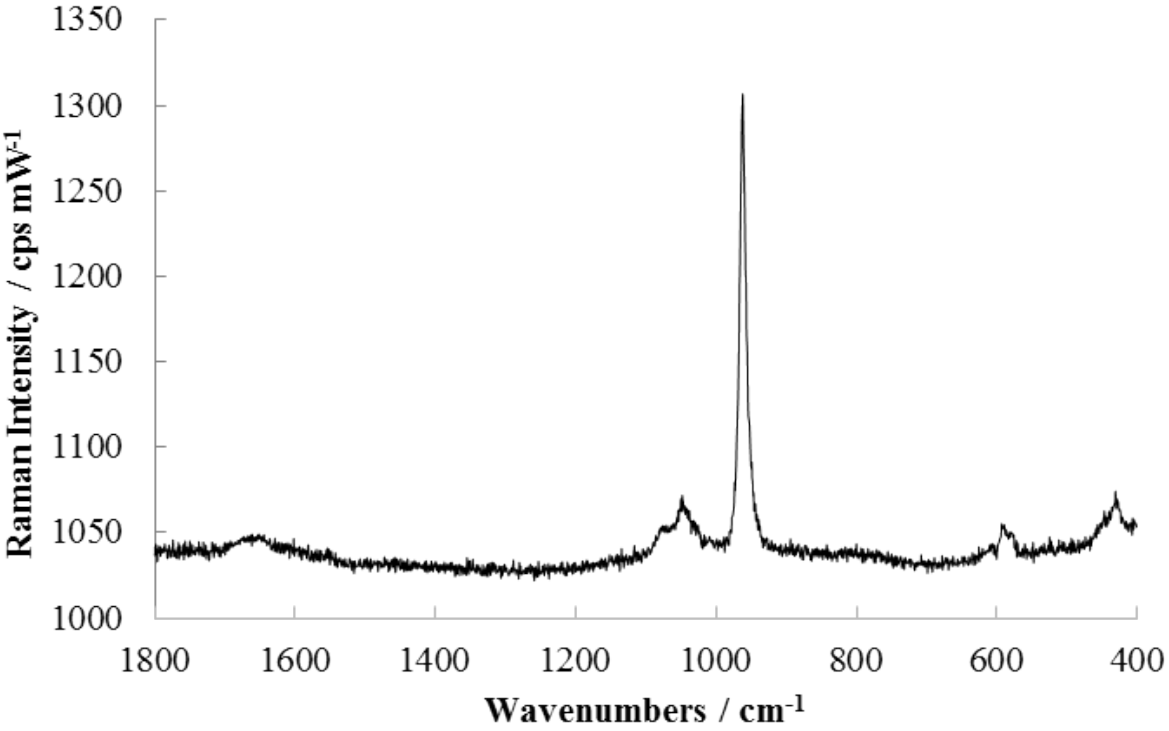

Figure 7. Raman spectrum of calcium phosphate tribasic.

4.1.2 Optimization of Bone Sample Spectra Collection

Raman spectra of bone were collected to elucidate differences between sample preparation (e.g. bone powder, cross sections, and excisions), laser wavelength, microscope objective, and grating to determine which yielded ideal spectral conditions. This experiment showed that the HeNe laser with the 600 groove/mm grating and the 100x objective was the best for resolving the large phosphate band at 960 cm^{-1} while at the same time limiting fluorescence. As depicted in Figure 8, human femur bone powder measured with the 100x objective exhibits much less fluorescence than with the 10x, and the baseline is better established since the broad underlying fluorescence band is lowered.

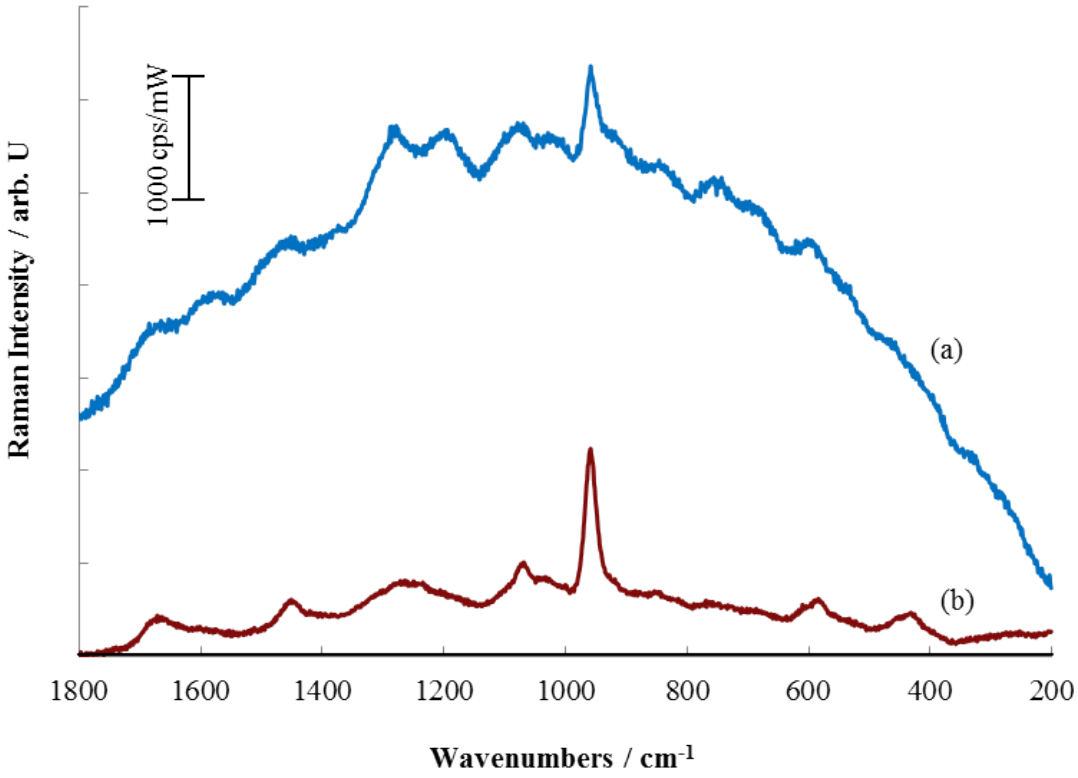

Figure 8. Raman spectra of femur bone powder using (a) 10x and (b) 100x microscope objectives.

4.1.3 Initial SERS with Bone Powder

Initial SERS trials were carried out to determine whether adding a silver nanoparticle suspension would enhance bands characteristic of human bone and possibly reduce the intensity of any bands that are not typically observed in the spectra of bone. One experiment that yielded promising results involved mixing silver particles (synthesized by the LM method) and powdered femur bone together in an arbitrary ratio. Figure 9 shows a plain powdered femur bone Raman spectrum and a powdered femur bone sample mixed with the LM silver particles. As seen in the literature spectrum of pure bone as well as the actual spectrum that was collected from femur powder, the small bands in the measured spectra at 450 cm^{-1} and 500 cm^{-1}, and the large band at 960 cm^{-1} that are observed in both spectra can be attributed

to the phosphate of the mineral component of bone. It can also be observed that while some of the other bands from bone are present in both spectra, many of the bands brought out by the silver particles are due to some other factor. In future projects, more spectra will be analyzed in order to investigate these new bands and gain a better understanding to which compounds they correspond.

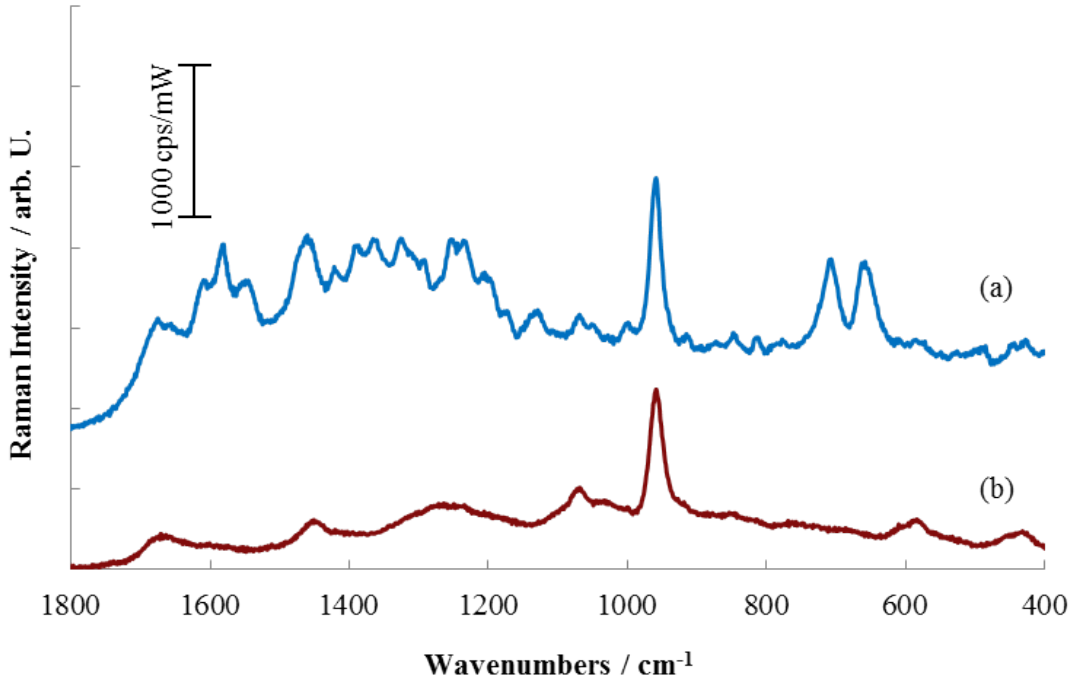

Figure 9. Raman spectra of (a) femur powder mixed with LM silver particles versus (b) plain femur powder.

4.2 Synthesis & Analysis of SERS Sandwich Substrates

The SERS substrate of choice for this research utilizes the interactions between silver particles and a smooth silver film to provide Raman enhancement. A smooth silver film is created by depositing silver on a glass surface that has been coated with a polymer to provide better adhesion of the film. After exposing the slides to more polymer, the substrates are placed into a silver nanoparticle suspension to create a top layer of silver nanoparticles. After the substrates are removed from the suspension and excess silver is rinsed away, they are dried

and a small amount of analyte can be directly pipetted onto the top layer and measured. These different layers create a "sandwich" of the analyte and different silver species whose SPPRs all interact to provide enhancement of the sample. An evaluation of these SERS substrates is presented in the following section and is based on characterizations of the various silver nanoparticle suspensions used for the nanoparticle layer, substrate appearance using SEM, and inter-slide and intra-slide Raman spectral reproducibility.

4.2.1 Ag Nanoparticle Synthesis & Characterization on Substrates

To investigate the effectiveness of silver nanoparticle size and inter-particle spacing on sandwich SERS substrates, several different silver nanoparticle suspensions were used as the top layer of the SERS sandwich substrates. Two major methods of silver suspension production were used: the hydrogen reduction method (suspensions A, B, and C) and the second by the Lee-Meisel citrate reduction method (suspension LM). The UV-Vis extinction spectrum of the LM particle suspension showed a dipole maximum at 406 nm (Figure 10) which is indicative of smaller particles than the hydrogen reduced suspensions A, B, and C, whose dipole maxima were at 430 nm, 491 nm, and 582 nm, respectively. SEM images of SERS substrates coated with the LM suspension, shown in Figure 10, revealed a polydispersed size distribution of particles.

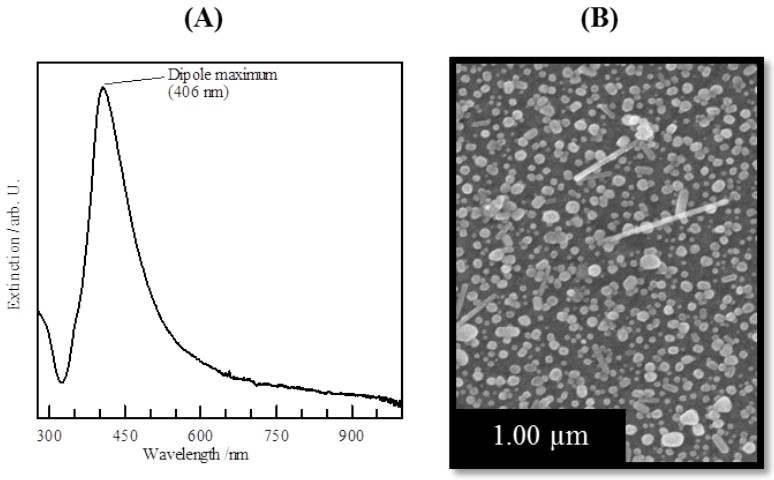

Figure 10. Characterization of the LM particles by (A) the extinction spectrum of the particles in suspension and (B) the SEM image of the particles on a SERS substrate.

The suspensions created by hydrogen reduction were obtained from work previously done by this lab and provided differently sized, monodispersed suspensions of silver particles, as shown in Figure 11. All of the substrates shown in the SEM images in Figures 10 and 11 were fabricated using silver nanoparticle suspensions that had an optical density (OD) of 10. Optical density is derived from the absorbance values at the dipole maximum for each silver suspension's extinction spectrum and is a relative value used to measure concentration.

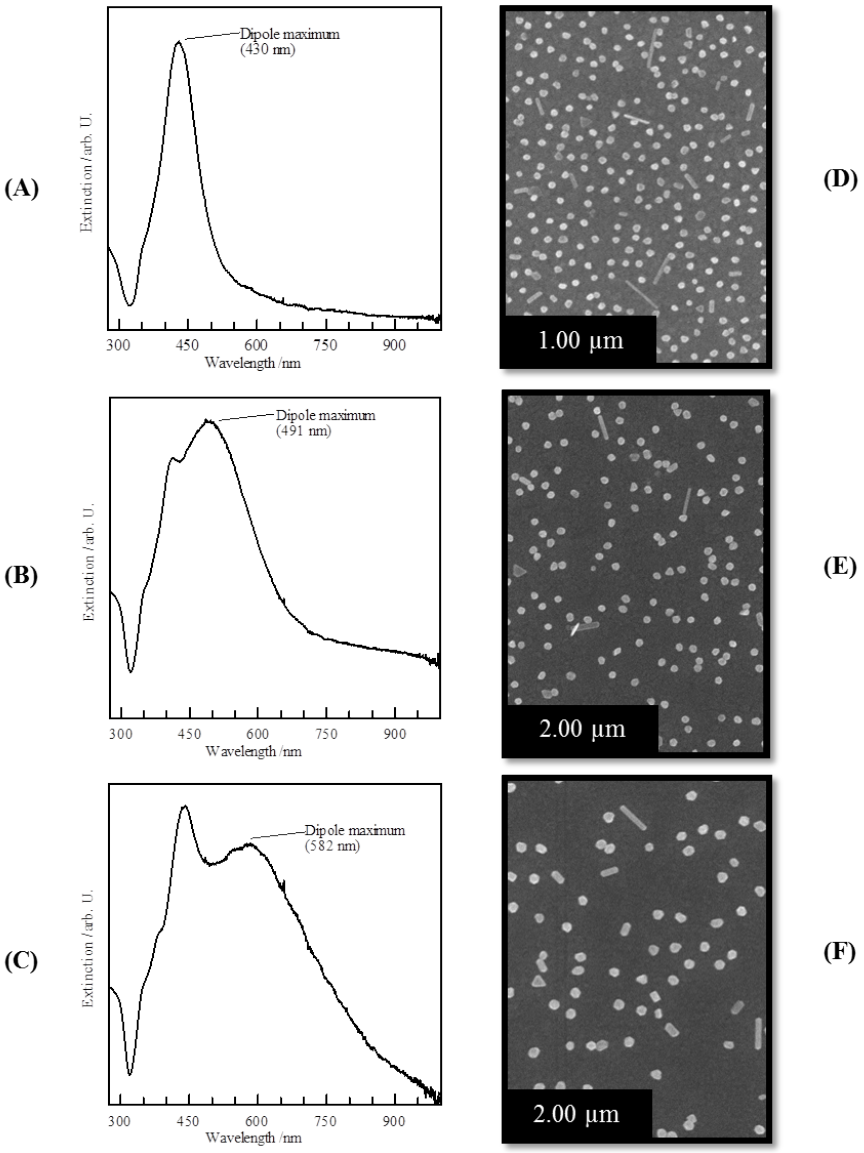

Figure 11. Characterization of H_2 reduced particles by the extinction spectra of (A) suspension A, (B) suspension B, and (C) suspension C. The SEM images of the particles on a SERS substrate are also shown for (D) suspension A, (E) suspension B, and (F) suspension C.

The dipole maxima from the extinction spectra of the suspensions, average particle size, and appearance of the different suspensions used with the SERS sandwich substrates are summarized in Table 1.

Table 1. Characteristics of different OD 10 Ag nanoparticle suspensions.

Ag Name	λ_{max} **(nm)**	**Average Particle Size (nm)**	**Appearance**
LM	406	46±20	polydispersed
A	430	51±4	monodispersed
B	491	103±8	monodispersed
C	582	141±11	monodispersed

4.2.2 Evaluation of Substrate Reproducibility

After the substrates were made, several initial experiments were carried out to determine the variability in SERS activity across a single substrate and between different locations on separate substrates. To accomplish this, spectra were collected at different positions on dried SERS substrates using the 100x microscope objective and 632.8 nm laser line with a 25% neutral density filter in place to avoid over-saturating the detector and/or degrading the substrate. The spectrum of each plain substrate was characteristic of the reference spectrum of PVP, which consists of a pyridine ring with a vinyl group attached in the position opposite the nitrogen of the ring. Characteristic bands of PVP can be observed in Figure 12 at 1010 cm^{-1}, and 1630 cm^{-1}, which are due to the aromatic ring vibrations of the pyridine and vibrations of the C=N functional group, respectively.[36] Some other less prominent bands that are observed in PVP are due to the alkene C=C and -CH_2- vibrational modes that are typically found between 1400 cm^{-1}-1900 cm^{-1}.

To test the intra-slide variation in acquired Raman spectra, the substrate was brought into focus and then measured at two different locations on the same slide. The resulting spectra were then normalized and subtracted from each other to produce a third spectrum indicative of only minuscule spectral changes across the substrate. To test the inter-slide variation in spectra, two substrates were brought into focus and then a different location was measured on each slide. These spectra were also normalized and subtracted, and also

revealed only minor variation across substrates. The spectra for these intra and inter-slide tests, along with the resulting subtracted spectra are shown in Figure 12.

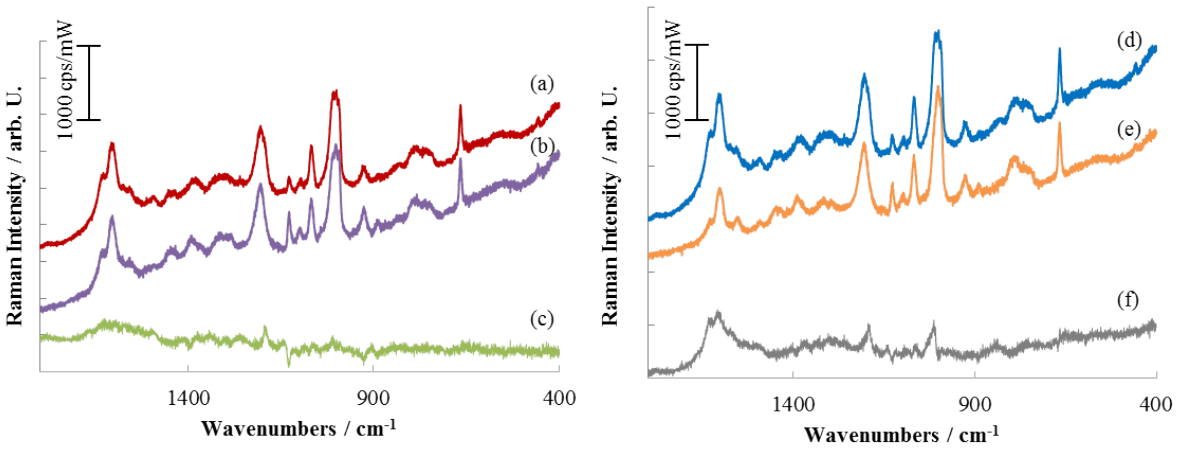

Figure 12. The variability of SERS activity across a single substrate and between different locations on separate substrates. Intra-slide variability was measured at two separate positions on the same slide (a & b), and inter-slide variability was measured at two positions on different slides (d & e). The differences in the spectra are also plotted for the intra-slide (c) and inter-slide (f) tests.

To further explore the reproducibility of the substrates, the imaging function on the LabSpec6 software was used to create a map of minor spectral differences over a small band range across a set location on a single substrate using two measurements at the same points. A 100 µm^2 box was outlined on the substrate image and spectra were collected at 36 individual points in the box. All spectra were collected using the 10x objective and a 1 second acquisition time with 25 accumulations. Since so many accumulations were collected and the entire scan took several hours, the SERS substrates were submerged in water to slow laser induced substrate degradation. The autofocus feature was used at each point to ensure that the initial image was in focus after each position change and that the maximum band height was achieved for each measurement. To achieve this, the autofocus was set to scan a range of 400 µm to determine the point at which the highest band intensity was obtained, which was considered to be the point at which the sample was in focus. Figure 13

shows images of an area on a single substrate after one (Figure 13A) and two (Figure 13B) mapping experiments were performed. Figures 13C and 13D show the resulting spectral color intensities that correspond to changes in intensity of the band at $1010\,\mathrm{cm}^{-1}$ in the substrate spectrum at each measurement point, where the lighter pixels represent where the band has the highest intensity. These two images show that there was not much of a change in intensity between the corresponding pixels of the two separate scans. Figure 13B indicates that a small amount of burning was taking place at each measurement point, but this destruction did not visually appear to influence the resulting intensity map in Figure 13D compared to Figure 13C.

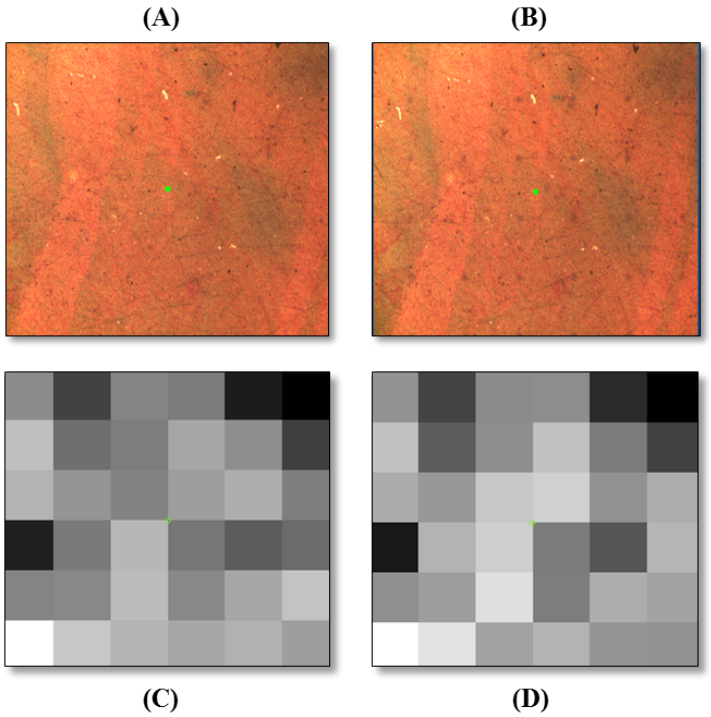

Figure 13. Chemical mapping across a section of a SERS substrate. Microscope images were taken after (A) one mapping experiment and (B) a second mapping experiment. A color map was created from the intensity changes of the largest band in the spectrum after (C) the first mapping experiment and (D) after the second mapping experiment.

4.3 Analysis of DNA & DNA Components

In this section, the Raman and SERS spectra of nucleotides were collected. Additionally, several optimization studies were carried out to see how varying the nanoparticle layer of the SERS substrate affected enhancement of the spectrum of the base adenine. The goal of these experiments was to generate Raman or SERS spectra of individual nucleotides of DNA, and then explore fabricating a substrate with optimal enhancement properties that would enable detection of low concentration of DNA.

4.3.1 Raman of DNA Base & Deoxyribose Powders

The Raman spectrum of each of the four DNA bases in powder form were collected using the 100x microscope objective with the 632.8 nm laser. Each spectrum was well resolved with little to no observable fluorescence. The molecular structure and corresponding spectrum of each base is shown in Figure 14. The same spectra are shown stacked in Figure 15 to show band locations of each base relative to each other. Table 2 was used to assign bands in spectra from each of the bases.[36] When comparing the base spectra, a trend emerges in some of the band placements due to the similar structure and functional groups present in each base. All four bases are heterocyclic amines which explains why all of the base spectra contain at least one band between 400 - 510 cm^{-1} and 1180 - 1280 cm^{-1} indicating C-N vibrations in the ring structures. The band found at 729 cm^{-1} for adenine and 651 cm^{-1} for guanine can be attributed to the purine rings of each of these substances. These bands are in the range between 650 - 900 cm^{-1} which corresponds to the out

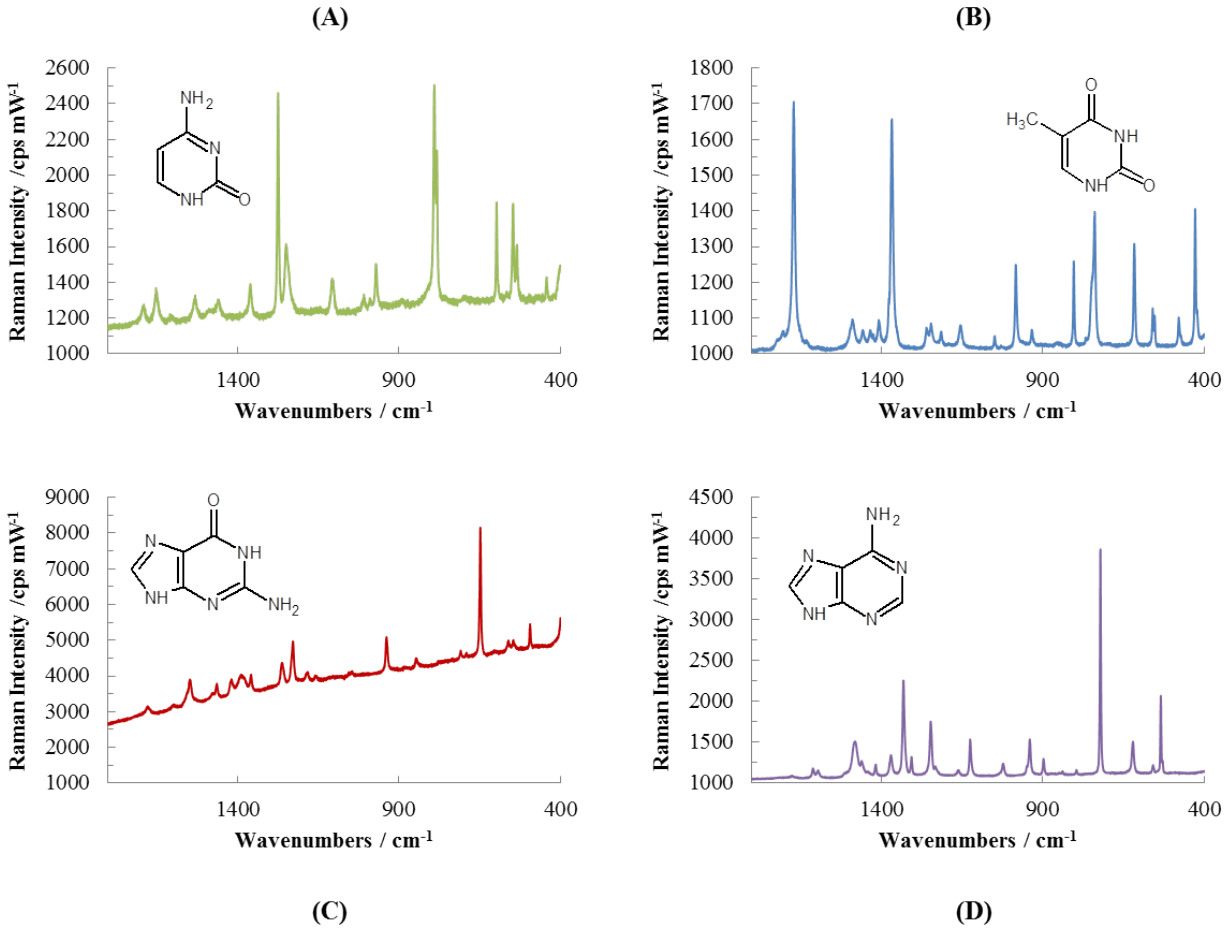

Figure 14. The structure and corresponding Raman spectra for the pyrimidines, (A) cytosine and (B) thymine, and the purines, (C) guanine and (D) adenine.

of plane bending mode of aromatic rings, and are much larger than that of the smaller, single ringed pyrimidines, cytosine and thymine. Also, all of the spectra exhibit a noticeable band between 1650 - 1800 cm^{-1}, which falls in the carbonyl band region and is due to the C=O stretching mode. Since adenine does not contain any carbonyl groups, there is no band present in this region for that substance.

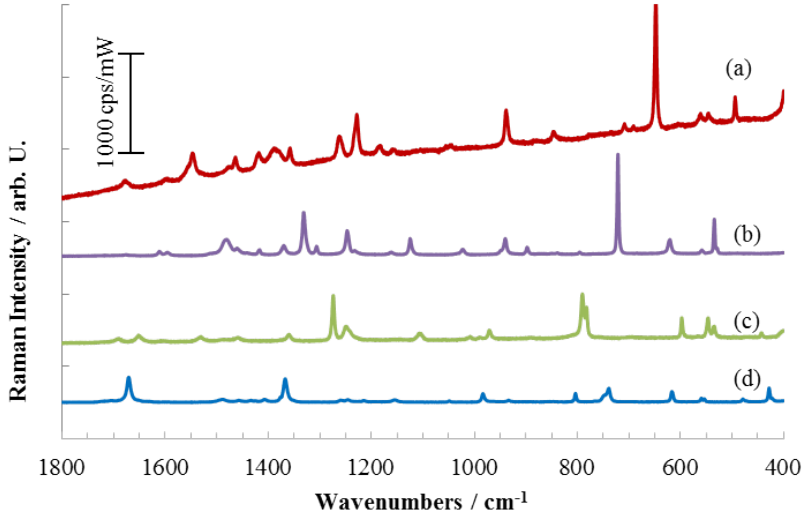

Figure 15. A comparison of band positions in the powder spectra of (A) guanine, (B) adenine, (C) cytosine, and (D) thymine.

Table 2. A specific representation of the Raman bands that are relevant to the vibrational modes found in DNA bases, nucleotides, and 2-deoxy-D-ribose.[36] ν indicates a stretching mode is being observed and δ represents a bending mode.

Functional Group/Vibration	**Region (cm^{-1})**
ν C=C	1900 - 1500
ν C=O	1800 - 1650
ν C=N	1680 - 1610
ν -CH_2-	1470 - 1400
ν P=O	1400 - 1175
ν C-N in amines	1350 - 1000
ν C-N in aromatic rings	1280 - 1180
ν (asym) C-O-C in ethers	1280 - 1060
ν C-O-C in ethers	970 - 800
δ (out of plane) aromatic rings	900 - 650
δ (out of plane) C=O in amides	615 - 535
δ C-N-C in amines	510 - 400

The spectrum of 2-deoxy-D-ribose powder, shown in Figure 16, was then collected using the same parameters as used for analyzing the base powders. The intense band at around 800 cm^{-1} and smaller bands between 1060 - 1280 cm^{-1} can be attributed to the symmetrical and asymmetrical stretching modes of the ether found in this compound. The second largest band in the spectrum at 1469 cm^{-1} is found in the region characteristic of -CH_2- groups, of which 2-deoxy-D-ribose contains two. It was also noted that the bands with the highest intensity in each spectra of both the base and 2-deoxy-D-ribose powders did not overlap with each other. This is promising because the presence of a band in future studies in any of these positions in the spectrum of a sample of bone could potentially indicate the presence of DNA.

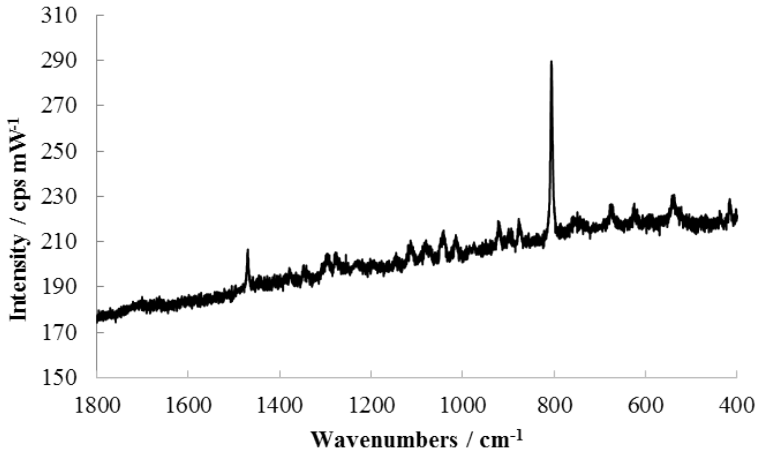

Figure 16. Raman spectrum of 2-deoxy-D-ribose powder.

4.3.2 Optimization of SERS Substrate Fabrication Parameters

As mentioned by previous research, it is believed that SERS sandwich substrates can utilize coupling from the interaction between particles and the smooth silver film as well as interactions between the particles themselves. In order to investigate the factors that lead to inter-particle coupling, several parameters were varied from the original sandwich SERS

substrate synthesis to try to affect inter-particle coupling. The difference in coupling related to the way the glass slides were cleaned was investigated by plasma cleaning or by rinsing with a 1:3 mixture of 30% H_2O_2/H_2SO_4 (piranha solution) prior to any further substrate fabrication steps. Another parameter that was varied with the substrates was the weight percent of PVP in solution (1% or 2% w/w) used to create the polymer sub-monolayers. Since the PVP monolayers must be heated near the glass transition phase of the polymer to become smoother, the annealing time (1 hour, 2 hours, or overnight) and annealing temperature (100 °C or 120 °C) were also varied. The addition of Na_2SO_4 salt and slide orientation during coating with silver particles were observed in order to investigate the effects related to position of the particles since these methods both affect inter-particle spacing.

To observe inter-particle coupling from these synthesis variations, PVP coated slides with no silver film were placed directly into a solution of silver nanoparticle suspension C after the changes to the fabrication method mentioned above were made. The slides were then measured using UV-vis spectroscopy to observe the extinction spectra of the silver particles adhered to the slide. The initial parameters that were tested were the concentration of PVP solution used to coat the slide, annealing time, and annealing temperature. The resulting spectra appeared to be very similar to that of the spectrum of the nanoparticle suspension, so it was determined that no large degree of coupling was achieved. Instead, the full width at half max (FWHM) of the large band in each spectrum was calculated to determine if there was any minute amount of coupling taking place. A table of this information is shown in Table 3. As a reference, the FWHM of nanoparticle suspension C with no substrate added was 341 nm. Table 3 shows that while there are minor changes in the FWHM values for the plasmon band in the extinction spectrum, there were no major observable trends in which parameters led to greater coupling. After this was determined, several other parameters were varied on top of the previously tested parameters from Table 3, including substrate cleaning method, the addition of a salt, and substrate coating orientation. These results were much

Table 3. An initial assessment of coupling by varying several substrate fabrication parameters including the resulting FWHM values.

PVP Concentration (%w)	**Anneal Temp. (°C)**	**Anneal Time (Hours)**	**FWHM**
1	120	12	246
1	100	12	172
1	120	2	204
1	100	2	266
1	120	1	197
1	100	1	188
2	120	12	198
2	100	12	213
2	120	2	214
2	100	2	206
2	120	1	183
2	100	1	212

more promising in that all resulting extinction spectra from substrates that were fabricated with the horizontal spin method indicated a significant amount of coupling, regardless of the other parameter changes. The FWHM values for a representative selection of the substrate where the second set of parameters were changed is shown in Table 4. These FWHM values show that the plasmon band is much narrower than with the vertical coating method. Figure 17 shows the extinction spectra using different coating methods with suspension C, which was the only variation made to the fabrication method that yielded a spectrum visibly indicative of inter-particle coupling. This figure aligns with previous research that determined that a particle array that exhibits coupling will have a Lorentzian-like curve in an extinction spectrum with a single, narrow band that corresponds to the absorbance maximum of the silver. As the particles get farther and farther apart the lack of constructive interference between particles causes the level of coupling to reduce and the extinction spectrum starts to resemble that of the extinction spectrum of the silver nanoparticle suspension.[35]

Table 4. A second assessment of coupling by varying several other substrate fabrication parameters including the resulting FWHM values.

PVP Conc. (%w)	Anneal Temp. (°C)	Anneal Time (Hours)	Salt Conc. (mM)	Cleaning Method	Coating Method	FWHM
1	100	12	0	Air Plasma	Horizontal	62
1	100	12	0	Air Plasma	Horizontal	58
1	100	12	0.75	Piranha Solution	Horizontal	58

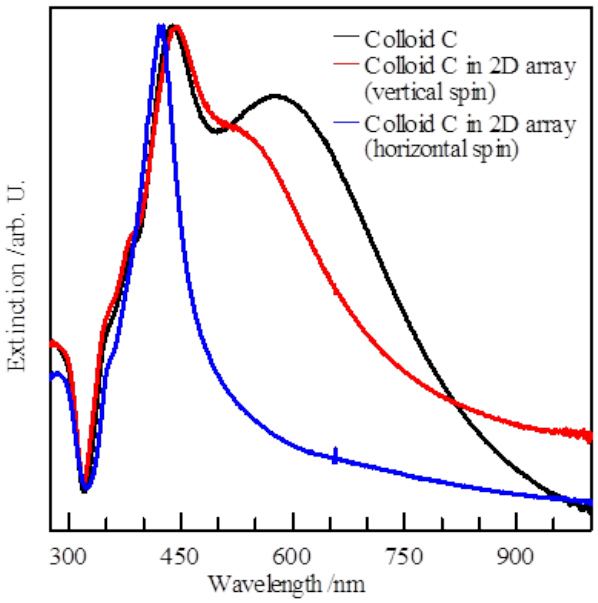

Figure 17. The extinction spectra of the nanoparticle suspensions adhered to PVP on plain glass to observe the effects of slide orientation during coating.

Likewise, the substrates that had been vertically attached to the rotisserie while immersed in silver suspension appeared to have extinction spectra that more closely resembled that of the plain silver suspension, while the horizontally assembled substrates yielded Lorentzian-like curves. The extinction spectrum of the substrate exposed to suspension C horizontally was identical to the spectra of the substrates where all of the other fabrication parameters mentioned were varied with a horizontal spin method. The extinction spectrum of the

substrate exposed to suspension C vertically was identical to the spectra of the substrates where all of the other fabrication parameters mentioned were varied and the spin method was vertical.

4.3.3 Optimization of SERS Substrates for Adenine Powder in Solution - A Limit of Detection Study

After the DNA base powders were measured, each powder was dissolved and measured as a solution. Adenine powder (0.50 g) was dissolved in NANOpure water and was sonicated to form a 0.15 M stock solution. The Raman spectrum of the resulting solution in shown in Figure 18. This spectrum shows a weak band at 1329 cm^{-1} that falls within the amine region where the vibrational stretching mode of C-N bonds are observed. The spectrum also shows a

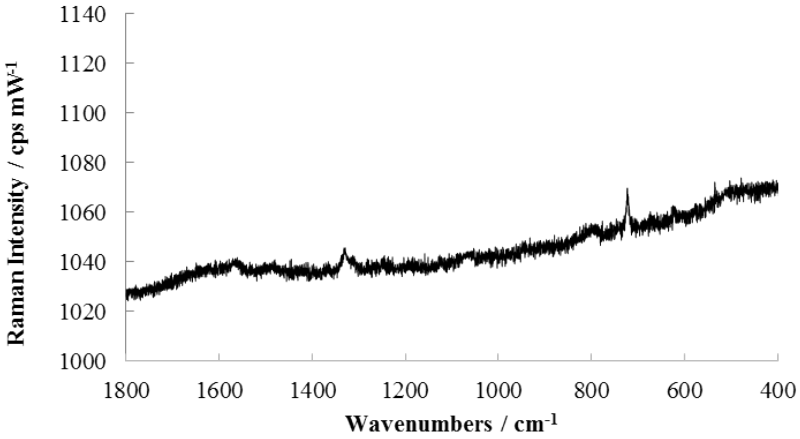

Figure 18. Raman spectrum of a concentrated 0.15 M aqueous solution of adenine

small band at 732 cm^{-1} that is the slightly shifted 729 cm^{-1} band that is characteristic of the out of plane bending of the aromatic ring in adenine powder. This band at 732 cm^{-1} was used to identify the presence or lack of adenine. Concentrated solutions of the other DNA bases were made, but with solvents that are incompatible with the SERS substrates. Guanine and

thymine, for instance, were insoluble in water, so the two were dissolved in separate solutions of the strong base, NH_4OH. The concentrated solutions were then measured using Raman with no observable spectra as a result. The solutions were then placed on a SERS substrate, whereupon immediate visible damage to the substrate occurred. The substrates are typically an orange hue under the Raman microscope, but in less than 30 seconds after exposure to the base solutions dissolved in NH_4OH the silver appeared to decompose to green with black areas of aggregation. An example of this decomposition is shown in Figure 19.

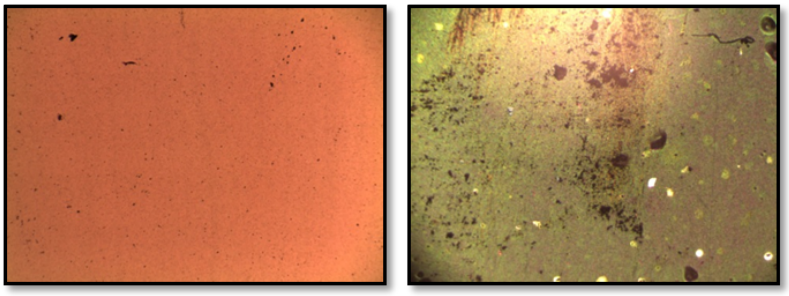

Figure 19. The resulting destruction of a SERS sandwich substrate (A) before and (B) after exposure to guanine dissolved in NH_4OH.

As discussed previously, the Raman spectrum of adenine dominates the spectrum of DNA, so it was not critical to this research to obtain reference spectra of the other bases. The dominance of adenine over thymine and cytosine is thought to be due to the extra Raman activity from the purine ring as opposed to the smaller pyrimidine rings. Adenine is also thought to dominate the spectrum of DNA over guanine because of the extra amine that adenine contains as opposed to the amide in guanine (Figure 14). Since a concentrated solution of adenine in a nondestructive solvent could be made, a series of 10-fold dilutions were made in order explore the limit of detection of adenine using different sandwich SERS substrate parameters. The three different aforementioned particle diameters from the syntheses using the hydrogen reduction method plus one particle diameter from the Lee-Meisel

particles were used to make four major categories of SERS-active substrates.

Several variations of these substrates were also made that investigated the effect on enhancement by using different concentrations of silver particle suspensions to form the particle arrays (OD 1, OD 5, OD 10, and OD 50), changing slide orientation while coating (vertical vs. horizontal), and adding salt to the particle suspension. The films were examined with a field emission scanning electron microscope (SEM) to determine the size distribution, shape, and aggregation state of the nanoparticles as shown in Section 4.2.1. The parameters of each individual substrate are shown below in Tables 5-8 and the corresponding stacked SERS spectra from each experiment are shown in Appendix A. Each of the following tables relates the parameters that were varied during the synthesis of the substrates such as the silver suspension (Ag ID), coating method, and OD. Several calculations are also included in the results tables that include the ordinate of the lowest adenine concentration that was detectable on the SERS substrate, the signal to noise ratio of the adenine band at $732\,\mathrm{cm}^{-1}$, the number of particles in the laser spot, and the analytical enhancement factor (AEF). The AEF was calculated from the equation:

$$AEF = \frac{I_{SERS}/C_{SERS}}{I_{samp}/C_{samp}} \tag{1}$$

where I is the area under the adenine band at $732\,\mathrm{cm}^{-1}$ and C is the concentration of the analyte in that particular measurement, and the subscript $SERS$ indicates the SERS sample while the subscript *samp* in the non-SERS measurement.

The first set of SERS sandwich substrate parameters that were explored was changing the OD of a single silver nanoparticle suspension. Table 5 shows that the largest four ODs yielded the greatest AEF values, but that they did not follow a linear trend since the OD 10 and OD 1 substrates yielded AEFs of an order of magnitude higher than that of OD 50 and OD 5. It should be noted though that the substrates with ODs that yielded the largest

enhancement factors of this entire SERS substrate study exhibited a shiny bluish tint that was not seen in any of the other substrate syntheses. It is predicted that some irreproducible, random factor is the cause of these large enhancement factors. It can also be concluded that the AEF appeared to be inversely proportional to the number of particles in the laser spot, which suggests that less particles leads to better enhancement.

Table 5. Limit of detection study using sandwich SERS substrates to observe the effect of using different nanoparticle concentrations by varying the concentration of nanoparticle suspension C used to coat the substrates.

Ag ID	**Coating Method**	**OD**	**Detectable Adenine (M)**	**S/N**	**Particles in Laser Spot (x10^6)**	**AEF (x10^4)**
C	vertical	50	10^{-7}	9.6	14 ± 2	420
C	vertical	10	10^{-8}	8.6	2.6 ± 0.3	4200
C	vertical	5	10^{-7}	52	12 ± 2	710
C	vertical	1	10^{-8}	8	3.4 ± 0.5	3800
C	vertical	0.01	10^{-6}	19	-	12

The next set of SERS sandwich substrate parameters that were explored was varying the silver suspension type used to coat the SERS sandwich substrates, both at high and low concentrations. Tables 6 and 7 summarize the results of each of the colloids A, B, C, and LM at ODs of 10 and 0.01. For the high concentration experiment, the OD was 10 but the actual concentration of the particle suspensions were calculated to be 1.33×10^{11} particles/mL, 3.9×10^{10} particles/mL, and 2.5×10^{10} particles/mL for suspensions A, B, and C, respectively. This is consistent with the increase in particle diameter between the suspensions because there are less of the larger suspension C particles in the same volume as the smaller A and B suspensions where more particles are present. Colloid C had the best AEF value suggesting that a larger sized monodispersed suspension is favorable. The LM particles showed the second largest AEF at this OD which suggests that the small population of large

Table 6. Limit of detection of adenine study using sandwich SERS substrates to observe the effect of Ag nanoparticle sizes on LOD by varying the nanoparticle suspension type at a high concentration.

Ag ID	**Coating Method**	**OD**	**Detectable Adenine (M)**	**S/N**	**Particles in Laser Spot (x10^6)**	**AEF (x10^4)**
A	vertical	10	10^{-6}	25	2.6 ± 0.1	63
B	vertical	10	10^{-7}	13	6.2 ± 1.0	240
C	vertical	10	10^{-8}	8.6	2.6 ± 0.3	4200
LM	vertical	10	10^{-7}	11	6.0 ± 1.2	400

particles in the polydispersed suspension are providing enhancement.

The low concentration of particles experiment yielded slightly concerning results when compared with the corresponding SEM images of these slides. For this experiment, the OD was 0.01 but the actual concentration of the particle suspensions were calculated to be 1.3×10^8 particles/mL, 3.9×10^7 particles/mL, and 2.4×10^7 particles/mL for suspensions A, B, and C, respectively. The enhancement factors for all of the different silver suspensions

Table 7. Limit of detection of adenine study using sandwich SERS substrates to observe the effect of Ag nanoparticle sizes on LOD by varying the particle suspension at a low concentration.

Ag ID	**Coating Method**	**OD**	**Detectable Adenine (M)**	**S/N**	**Particles in Laser Spot (x10^6)**	**AEF (x10^4)**
A	vertical	0.01	10^{-6}	9.9	-	9.6
B	vertical	0.01	10^{-6}	27	-	13
C	vertical	0.01	10^{-6}	19	-	12
LM	vertical	0.01	10^{-7}	9.8	-	130

were relatively low compared to other studies in this project, but they were still rather large in that the lowest was still four orders of magnitude higher than the non-enhanced concentrated

adenine solution. This is concerning because the SEM images showed that there were none of the silver nanoparticles on the slide, but rather, randomly and sparsely dispersed aggregates of silver. This would suggest that perhaps the saturated silver oxide solution was the only thing adhering to these low concentration slides, but the aggregates of this solution were enough to provide a large amount of enhancement compared to non-enhanced Raman.

The next parameter that was tested was coupling between silver nanoparticles. In order to force the particles closer together than they would randomly assemble, adding a salt, such as sodium sulfate, in low concentrations has been experimentally shown to achieve this and lead to particle coupling.[31] The effects of coupling were only tested with silver suspension C due to the scarcity of the other hydrogen reduced colloids, and the results are shown in Table 8. After mixing a portion of the particles with Na_2SO_4, the resulting suspension was

Table 8. Limit of detection of adenine study using sandwich SERS substrates to observe the effect of inter-particle coupling on LOD by adding 0.75 M $NaNO_3$ salt to particle suspension C.

Ag ID	**Coating Method**	**OD**	**Detectable Adenine (M)**	**S/N**	**Particles in Laser Spot (x10^6)**	**AEF (x10^4)**
C (+salt)	horizontal	50	10^{-5}	23	43 ± 2	7.1
C	horizontal	50	10^{-5}	29	13 ± 0.4	3.4

characterized using UV-vis and was compared to suspension C without salt. The resulting UV-vis spectrum after the addition of salt was identical to the original suspension with no salt. The SEM images of the substrates coated with the C suspension with salt (Figure 20B) showed a large increase in the number of silver particles compared to suspension C with no salt (Figure 20A). The resulting effects on the enhancement of adenine in solution were unexpectedly small considering the large increase in number of nanoparticles in the laser spot. However, according to the experiments summarized in Table 4, the addition of salt

did not have a noticeable impact on the FWHM of the plasmon band indicating no further increase in coupling.

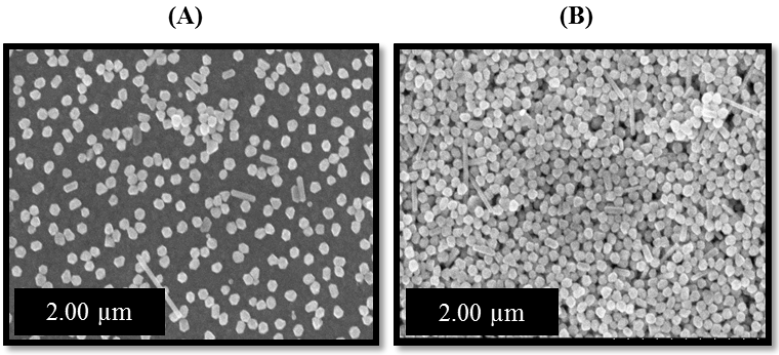

Figure 20. SEM images of SERS sandwich substrates coated with (A) Ag suspension C without salt and (B) Ag suspension C with salt.

The last parameter to be tested was the effect of slide orientation while on the rotisserie in the polymer and silver suspension phases of synthesis. As discussed previously, it was determined through much trial and error that by simply attaching the vial containing the substrate to the rotisserie in a horizontal manner, rather than the conventional vertical orientation, coupling could be observed in the resulting substrates. These parameters were

Table 9. Limit of detection study using sandwich SERS substrates to observe the effect of substrate coating orientation by varying the spin method.

Ag ID	**Coating Method**	**OD**	**Detectable Adenine (M)**	**S/N**	**Particles in Laser Spot ($\times 10^6$)**	**AEF ($\times 10^4$)**
B	vertical	10	10^{-7}	13	6.3 ± 1.0	240
B	horizontal	10	10^{-6}	92	8.0 ± 0.4	110
C	vertical	50	10^{-7}	9.6	14 ± 2	420
C	horizontal	50	10^{-5}	29	13 ± 0.4	3.4

used to fabricate SERS substrates in order to determine if this type of coupling would lead to any further enhancement of adenine in solution. Table 9 shows that coupling with suspension

B yielded a small change in AEF, while coupling with suspension C yielded a much lower AEF than the non-coupling conventional vertical coating method.

4.3.4 SERS of Nucleotide Solutions & DNA

After seeing promising results of low concentrations of adenine solutions, a dATP nucleotide solution (100 mM) was measured on a SERS substrate using the original substrate synthesis parameters that used suspension B at OD 10 with a vertical spin method and no salt added.[28] Figure 21 shows the resulting spectrum that was dominated by the PVP background spectrum of the SERS substrate, but a small band was distinguishable at 732 cm^{-1}. This band was established in the experiments with adenine powder in solution as being indicative of adenine, and was not present in the background spectrum of the substrate. Since nucleotides contain phosphate bonds, there was expected to be a band present 1175 - 1400 cm^{-1}, but there was no such band that was distinguishable from the bands already present in the PVP spectrum.

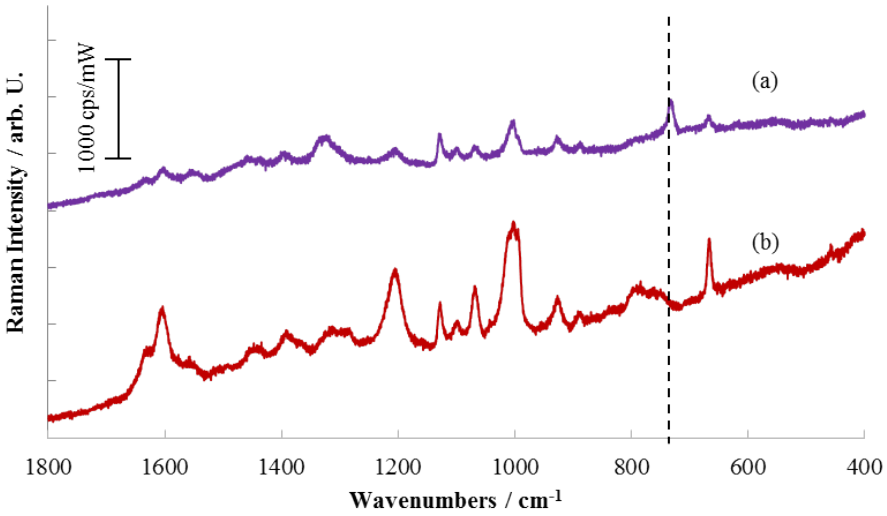

Figure 21. SERS spectrum of (a) a dATP nucleotide solution on a sandwich SERS substrate and (b) the background spectrum of water on the same sandwich substrate.

The spectrum of a sample of control DNA ($10\,\mathrm{ng/\mu L}$), which was calculated to contain around $8 \times 10^{-6}\,\mathrm{M}$ adenine, was measured using the same original substrate synthesis method, but no bands other than that of the substrate background were observed. While the concentration of adenine in this DNA suspension was lower than the concentration of adenine in an adenine solution detected by the same substrate ($10^{-7}\,\mathrm{M}$), the adenine band was not detected. The absence of the $732\,\mathrm{cm}^{-1}$ band was thought to be due to the possibility that the DNA is orientated in such a way that the bound adenine is too far away from the silver surface of the substrates.

CHAPTER 5: CONCLUSION & FUTURE DIRECTIONS

The groundwork for determining whether Raman Spectroscopy and SERS is a useful technique as a pre-extraction technique for the detection of DNA in various substrates has been successfully initiated. Several Raman spectra of bone and DNA components were collected and the optimal parameters with Western Carolina University's Raman spectrometer, Raman microscope, and associated lasers for bone and DNA component samples were successfully determined. It was also determined experimentally that adenine, a purine base found in DNA, is the only nucleobase that is detectable by Raman spectroscopy in a concentrated aqueous solution, and it's detection is also easily enhanced by several orders of magnitude using sandwich SERS substrates. The detection of the band attributed to the aromatic ring found in adenine at $732\,\mathrm{cm}^{-1}$ in many low concentration aqueous solutions of adenine was successful down to $10^{-8}\,\mathrm{M}$. While this band was also detected in a solution of the nucleotide dATP, the presence of the band was not observed in a $10\,\mathrm{ng/\mu L}$ DNA suspension. Given that the limit of detection of the substrate used was lower than that of the concentration of adenine in the DNA sample, it is thought that the adenine in the DNA is oriented in such a fashion that it is too far away from the silver surface to undergo significant enhancement. A future experiment to test this hypothesis would be to use single stranded DNA to attempt to understand the adsorption of the DNA to the silver surface.

Several parameters for the fabrication and optimization of the sandwich SERS substrates were investigated and preliminary results and trends were noted. Previous research suggests that more coupling present on a sandwich SERS substrate from various inter-particle and particle-film sources leads to even larger enhancement than when just one type of coupling is present. However, the initial research that has been carried out in the project suggests the opposite. It was determined in this research that inter-particle coupling is easily achieved on the sandwich SERS substrates by simply changing the orientation of the substrate while

being exposed to a silver nanoparticle suspension. The AEF values for solutions of adenine on the SERS substrates were highest when factors that led to inter-particle coupling were not carried out. It is hypothesized that the more coupled particles - whether derived from a horizontal spin method or the addition of salt - encounter too much destructive interference from all of the various SPPRs and actually end up with less of an ability to enhance the signal of an analyte molecule in close proximity. To further investigate the enhancement effects of different types of coupling, more sandwich SERS substrates will be fabricated on a larger scale to confirm that the trends in inter-particle coupling shown in this research are reproducible.

Since the foundation has been laid for the use of these optimized sandwich SERS substrates for the detection of adenine, and by extension DNA, the next steps that will be taken in future research will be to further optimize these substrates for the detection of low quantities of adenine in DNA. The detection of adenine in DNA samples is key to the main application of this research, as it is desired to find a substrate that will aim to detect small changes in the adenine band that could potentially be related to degradation of DNA in a sample. After DNA is detected, experiments can be directed towards detecting the adenine found in DNA in various media, such as bones. Another step further in the future would be to expose bones to different factors (e.g. weather, chemicals, etc.) to determine how Raman spectral changes relate to DNA degradation through changes in the band that correlates to adenine.

REFERENCES

[1] Hochmeister, M. N.; Budowle, B.; Borer, U. V.; Eggmann, U.; Comey, C. T.; Dirnhofer, R. *J. Forensic Sci.* **1991**, *36*, 1649–1661.

[2] Salamon, M.; Tuross, N.; Arensburg, B.; Weiner, S. *Proc. Natl. Acad. Sci. U.S.A.* **2005**, *102*, 13783–8.

[3] Morris, M. D.; Mandair, G. S. *Clin. Orthop. Relat. Res.* **2011**, *469*, 2160–9.

[4] Havaldar, R.; Pilli, S. C.; Putti, B. B. *Journal of Dental and Medical Sciences* **2012**, *1*, 12–16.

[5] Chang, S. W.; Shefelbine, S. J.; Buehler, M. J. *Biophys. J.l* **2012**, *102*, 640–648.

[6] Adler, C. J.; Haak, W.; Donlon, D.; Cooper, A. *J. Archaeol. Sci.* **2011**, *38*, 956–964.

[7] Martin, R. Bones: Structure and Mechanics. 2003.

[8] Koester, K. J.; Barth, H. D.; Ritchie, R. O. *J. Mech. Behav. Biomed. Mater.* **2011**, *4*, 1504–1513.

[9] Donnelly, E.; Meredith, D. S.; Nguyen, J. T.; Boskey, A. L. *J. Orthop. Res.* **2012**, *30*, 700–706.

[10] Barhoumi, A.; Zhang, D.; Tam, F.; Halas, N. J. *J.Am. Chem. Soc.* **2008**, *130*, 5523–9.

[11] Ager, J. W.; Nalla, R. K.; Breeden, K. L.; Ritchie, R. O. *J. Biomed. Opt.* **2005**, *10*, 34012.

[12] Lakshmi, R. J.; Alexander, M.; Kurien, J.; Mahato, K. K.; Kartha, V. B. *Appl. Spectrosc.* **2003**, *57*, 1100–1116.

[13] Callender, A. F.; Finney, W. F.; Morris, M. D.; Sahar, N. D.; Kohn, D. H.; Kozloff, K. M.; Goldstein, S. A. *Vib. Spectrosc.* **2005**, *38*, 101–105.

[14] De Carmejane, O.; Morris, M. D.; Davis, M. K.; Stixrude, L.; Tecklenburg, M.; Rajachar, R. M.; Kohn, D. H. *Calcif. Tissue Int.* **2005**, *76*, 207–213.

[15] Ebersberger, I.; Metzler, D.; Schwarz, C.; Pääbo, S. *Am. J. Hum. Genet.* **2002**, *70*, 1490–1497.

[16] Carpi, F. M.; Di Pietro, F.; Vincenzetti, S.; Mignini, F.; Napolioni, V. *Recent patents on DNA & gene sequences* **2011**, *5*, 1–7.

[17] Simbolo, M.; Gottardi, M.; Corbo, V.; Fassan, M.; Mafficini, A.; Malpeli, G.; Lawlor, R. T.; Scarpa, A. *PLoS ONE* **2013**, *8*.

[18] Utzinger, U.; Richards-Kortum, R. R. *J. Biomed. Opt.* **2003**, *8*, 121–147.

[19] Zavaleta, C. L.; Kircher, M. F.; Gambhir, S. S. *J. Nucl. Med.* **2011**, *52*, 1839–1844.

[20] Kneipp, K.; Kneipp, H.; Itzkan, I. *Chem. Rev.* **1999**, *99*, 2957–2976.

[21] Fleischmann, M.; Hendra, P. J.; McQuillan, A. J. *Chem. Phys. Lett.* **1974**, *26*, 163–166.

[22] Hudson, S. D.; Chumanov, G. *Anal. Bioanal. Chem.* **2009**, *394*, 679–686.

[23] Pearman, W. F.; Fountain, A. W. *Appl. Spectrosc.* **2006**, *60*, 356–365.

[24] Primera-Pedrozo, O. M.; Jerez-Rozo, J. I.; De La Cruz-Montoya, E.; Luna-Pineda, T.; Pacheco-Londoño, L. C.; Hernández-Rivera, S. P. *IEEE Sens. J.* **2008**, *8*, 963–973.

[25] Jarvis, R. M.; Goodacre, R. *Chem. Soc. Rev.* **2008**, *37*, 931–936.

[26] Evanoff, D. D.; Chumanov, G. *Chemphyschem* **2005**, *6*, 1221–31.

[27] Cialla, D.; März, A.; Böhme, R.; Theil, F.; Weber, K.; Schmitt, M.; Popp, J. *Anal. Bioanal. Chem.* **2012**, *403*, 27–54.

[28] Daniels, J. K.; Chumanov, G. *J. Phys. Chem. B* **2005**, *109*, 17936–17942.

[29] Lee, P. C.; Meisel, D. *J. Phys. Chem.* **1982**, *86*, 3391–3395.

[30] Evanoff, D. D.; Chumanov, G.; Evanoff Jr., D. D. *J. Phys. Chem. B* **2004**, *108*, 13957–13962.

[31] Kinnan, M. K.; Chumanov, G. *J. Phys. Chem. C* **2010**, *114*, 7496–7501.

[32] Malynych, S.; Chumanov, G. *J. Am. Chem. Soc.* **2003**, *125*, 2896–2898.

[33] Pinchuk, A. O.; Schatz, G. C. *Mater. Sci. Engr. B* **2008**, *149*, 251–258.

[34] Jang, L.-W.; Jeon, D.-W.; Kim, M.; Jeon, J.-W.; Polyakov, A. Y.; Ju, J.-W.; Lee, S.-J.; Baek, J.-H.; Yang, J.-K.; Lee, I.-H. *Adv. Funct. Mater.* **2012**, *22*, 2728–2734.

[35] Pinchuk, A. O.; Schatz, G. C. *Appl. Phys. B: Lasers Opt.* **2008**, *93*, 31–38.

[36] Lambert, J. B.; Shurvell, H. F.; Cooks, R. G. *Introduction to Organic Spectroscopy*; 1987; pp 174–177.

APPENDIX A: SERS SPECTRA FOR THE DETECTION OF ADENINE

The following SERS spectra were collected with a 1 second integration with 3 averages using the 632.8 nm HeNe laser and the 10x microscope objective. For each substrate, four spectra were collected:(a) a 3.5×10^{-3} M aqueous adenine solution, (b) the lowest concentration of adenine that yielded the characteristic band at 732 cm^{-1} as indicated in Tables 2-6, (c) an adenine solution that is one order of magnitude lower in concentration than the solution in b to show that the adenine band vanished, and (d) the spectrum of plain water on each individual SERS substrate. Each set of spectra is labeled with the Ag suspension ID, the OD, and the coating method that was used to synthesize the corresponding SERS substrate.

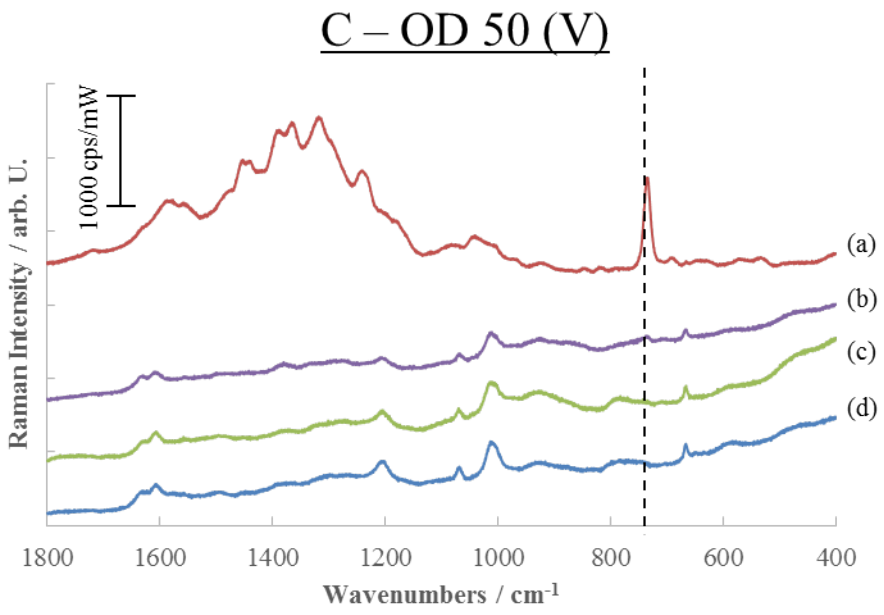

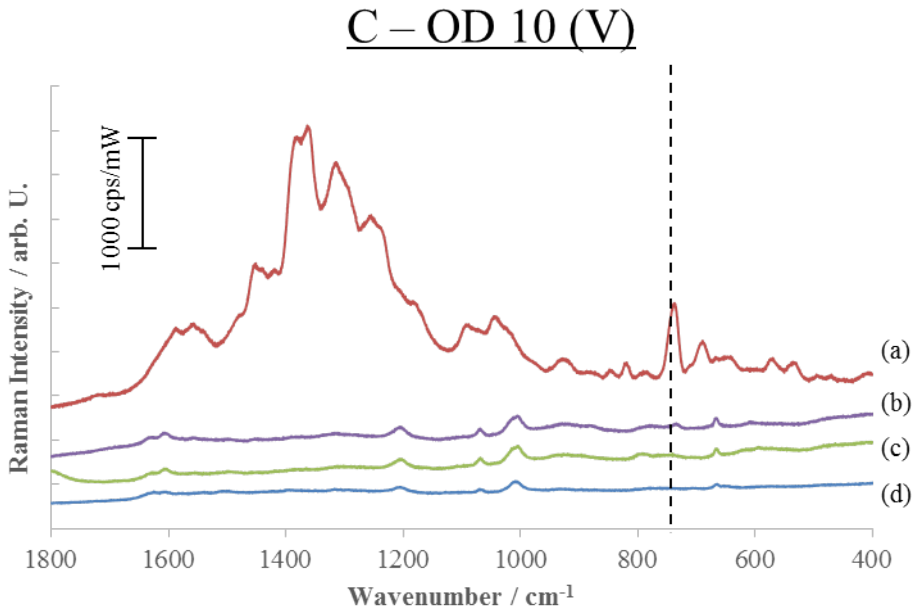
C – OD 10 (V)
1000 cps/mW
Raman Intensity / arb. U.
(a)
(b)
(c)
(d)
1800
1600
1400
1200
1000
800
600
400
Wavenumber / cm-1

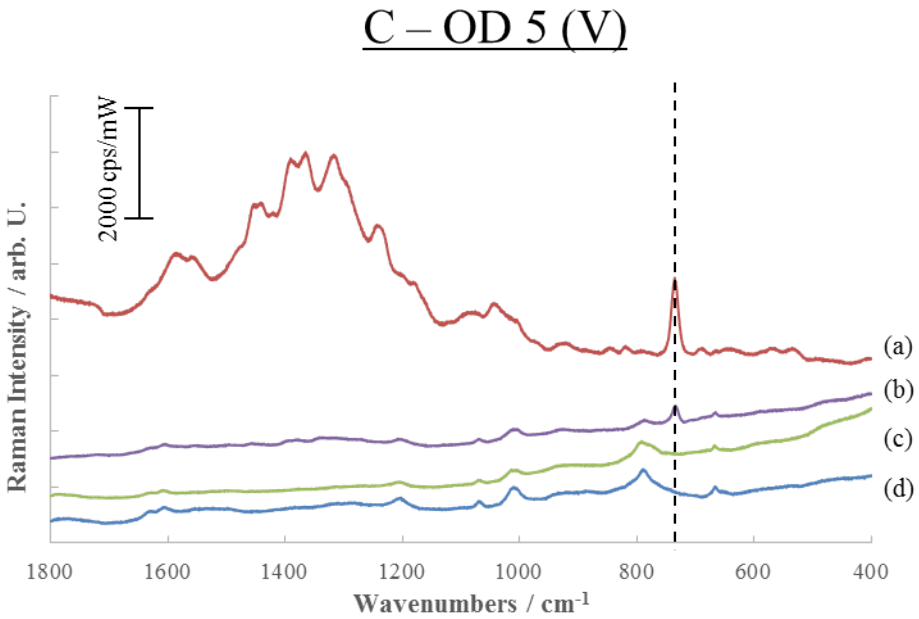
C – OD 5 (V)
2000 cps/mW
Raman Intensity / arb. U.
(a)
(b)
(c)
(d)
1800
1600
1400
1200
1000
800
600
400
Wavenumbers / cm-1

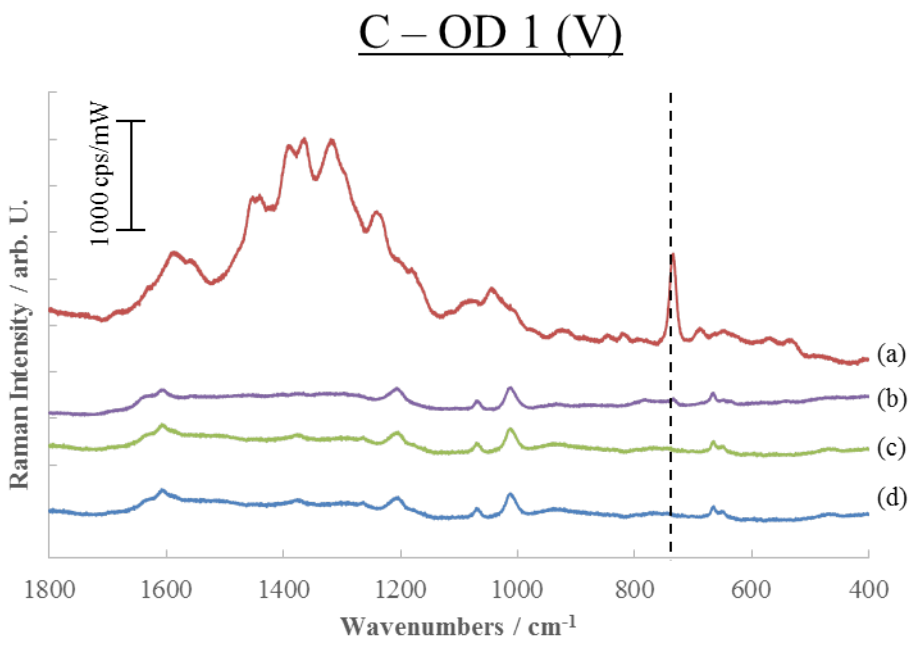
C – OD 1 (V)
1000 cps/mW
Raman Intensity / arb. U.
(a)
(b)
(c)
(d)
1800
1600
1400
1200
1000
800
600
400
Wavenumbers / cm-1

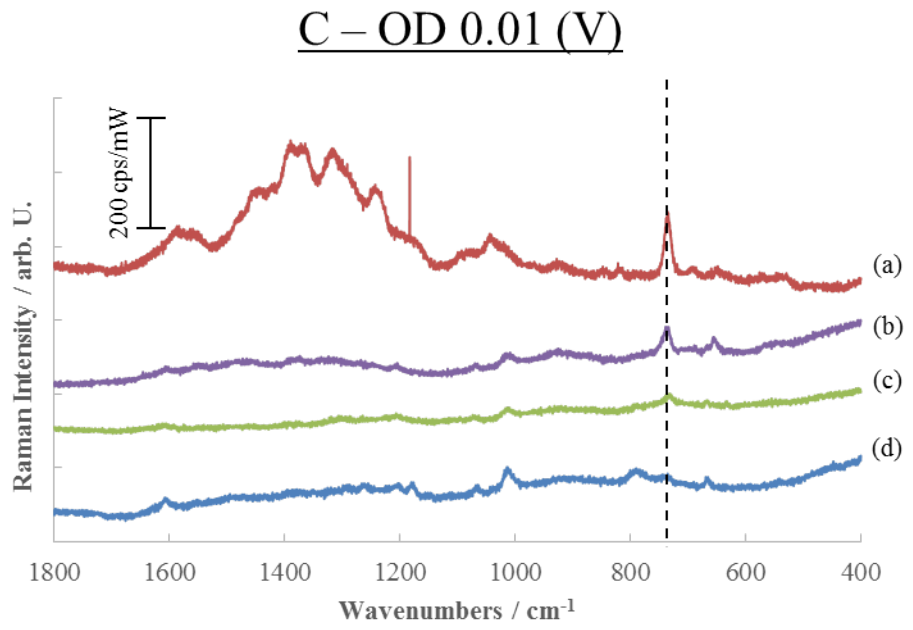
C – OD 0.01 (V)
200 cps/mW
Raman Intensity / arb. U.
(a)
(b)
(c)
(d)
1800
1600
1400
1200
1000
800
600
400
Wavenumbers / cm-1

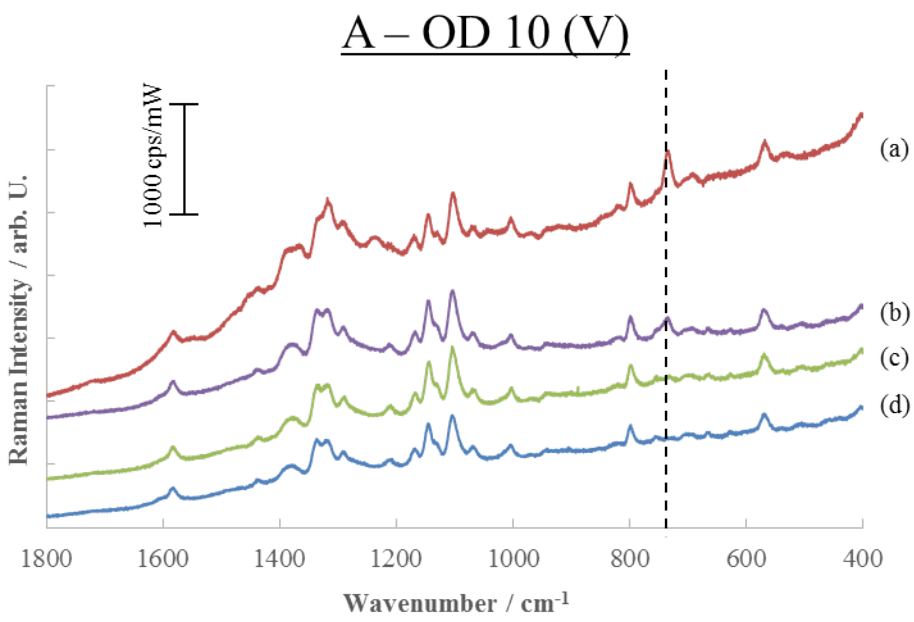
A – OD 10 (V)
1000 cps/mW
Raman Intensity / arb. U.
(a)
(b)
(c)
(d)
1800
1600
1400
1200
1000
800
600
400
Wavenumber / cm-1

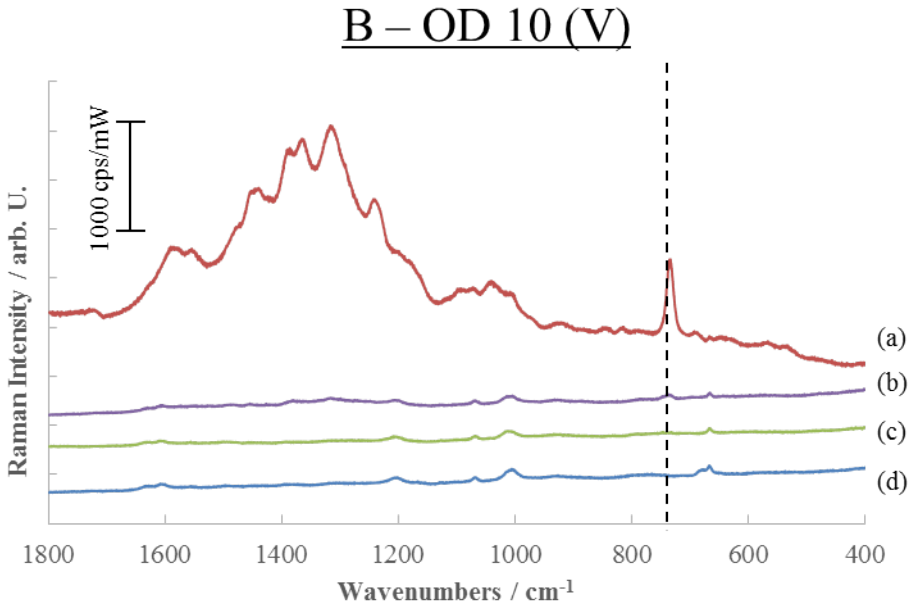
B – OD 10 (V)
1000 cps/mW
Raman Intensity / arb. U.
(a)
(b)
(c)
(d)
1800
1600
1400
1200
1000
800
600
400
Wavenumbers / cm-1

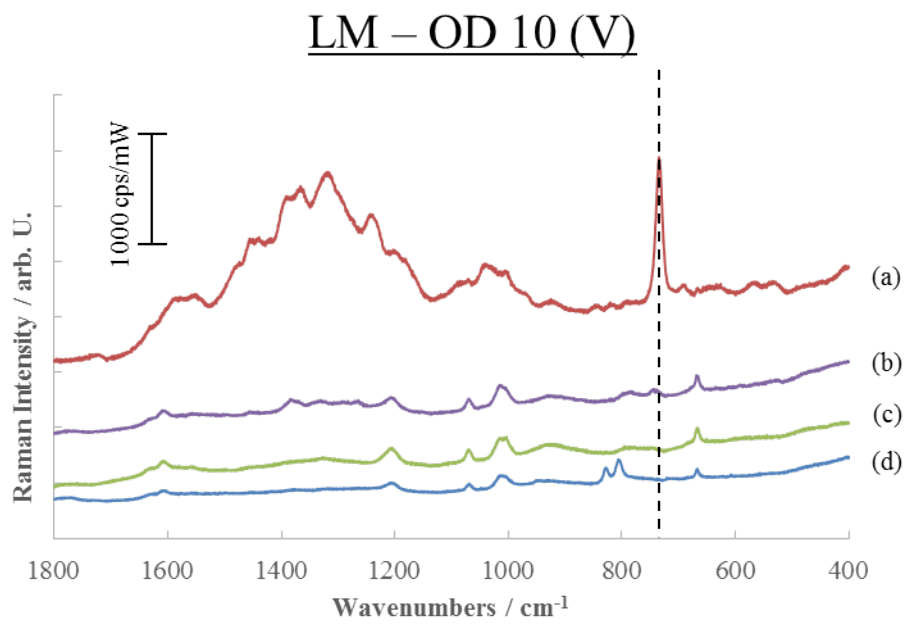
LM – OD 10 (V)
1000 cps/mW
Raman Intensity / arb. U.
(a)
(b)
(c)
(d)
1800
1600
1400
1200
1000
800
600
400
Wavenumbers / cm-1

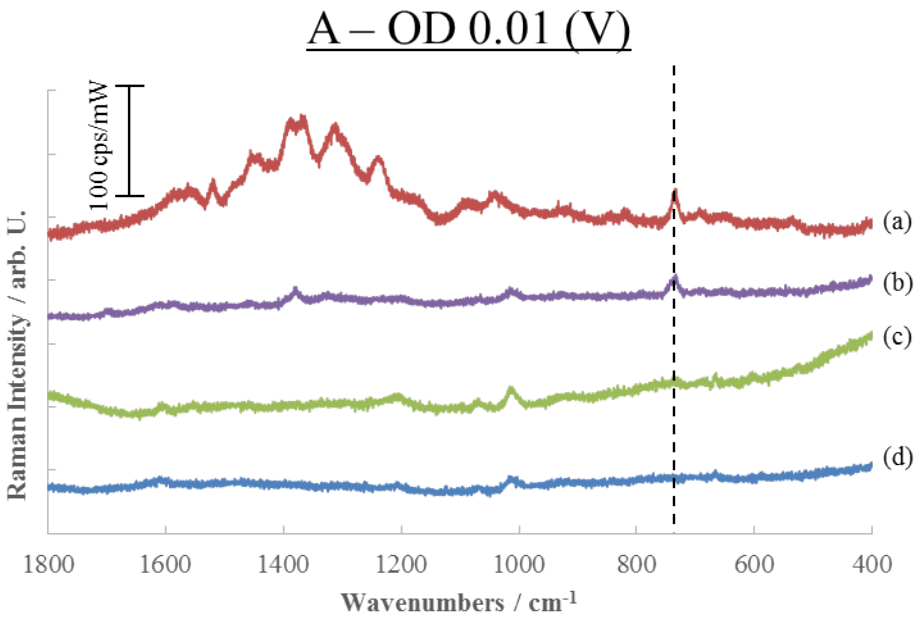
A – OD 0.01 (V)
100 cps/mW
Raman Intensity / arb. U.
(a)
(b)
(c)
(d)
1800
1600
1400
1200
1000
800
600
400
Wavenumbers / cm-1

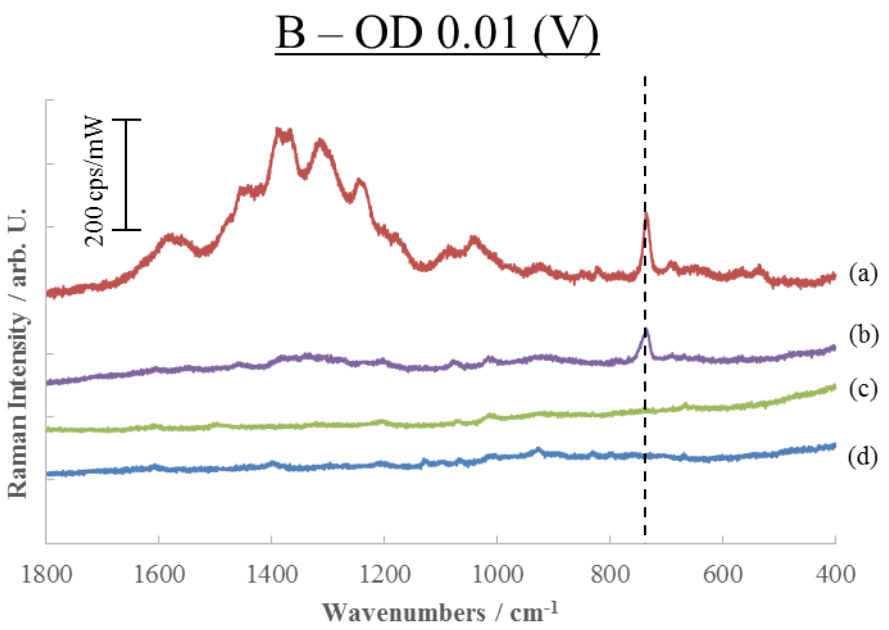
B – OD 0.01 (V)
200 cps/mW
Raman Intensity / arb. U.
(a)
(b)
(c)
(d)
1800
1600
1400
1200
1000
800
600
400
Wavenumbers / cm-1

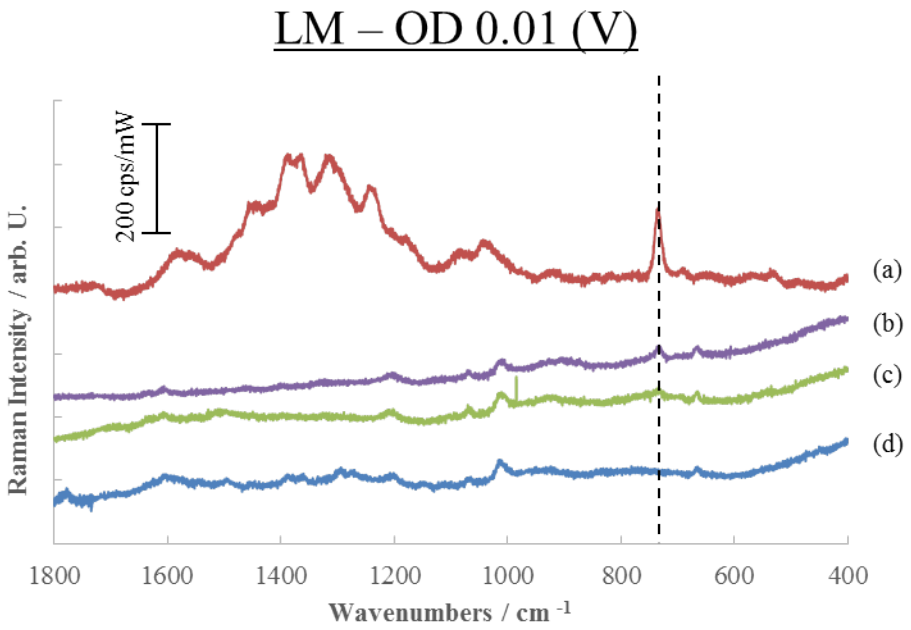
LM – OD 0.01 (V)
200 cps/mW
Raman Intensity / arb. U.
(a)
(b)
(c)
(d)
1800
1600
1400
1200
1000
800
600
400
Wavenumbers / cm -1

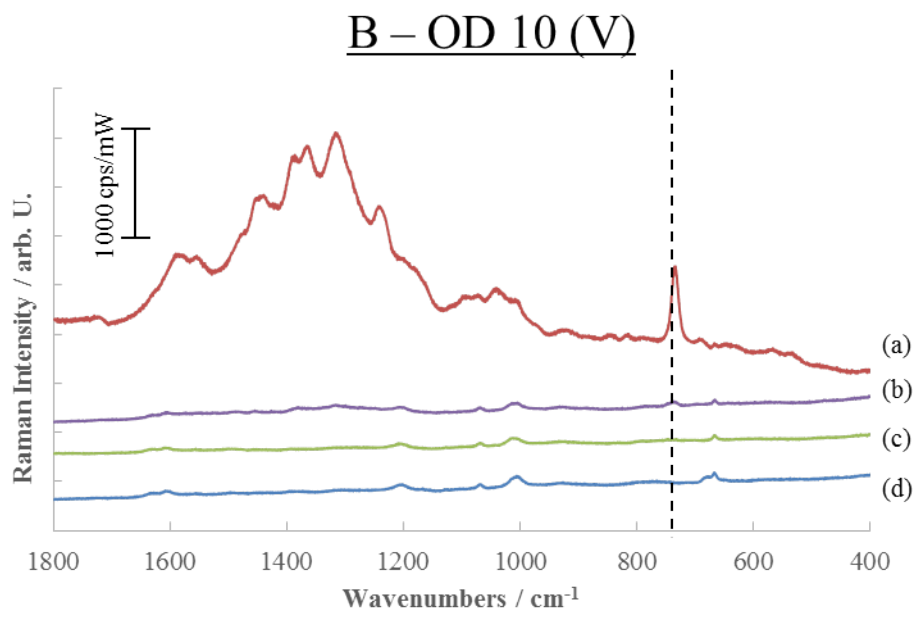
B – OD 10 (V)
1000 cps/mW
Raman Intensity / arb. U.
(a)
(b)
(c)
(d)
1800
1600
1400
1200
1000
800
600
400
Wavenumbers / cm-1

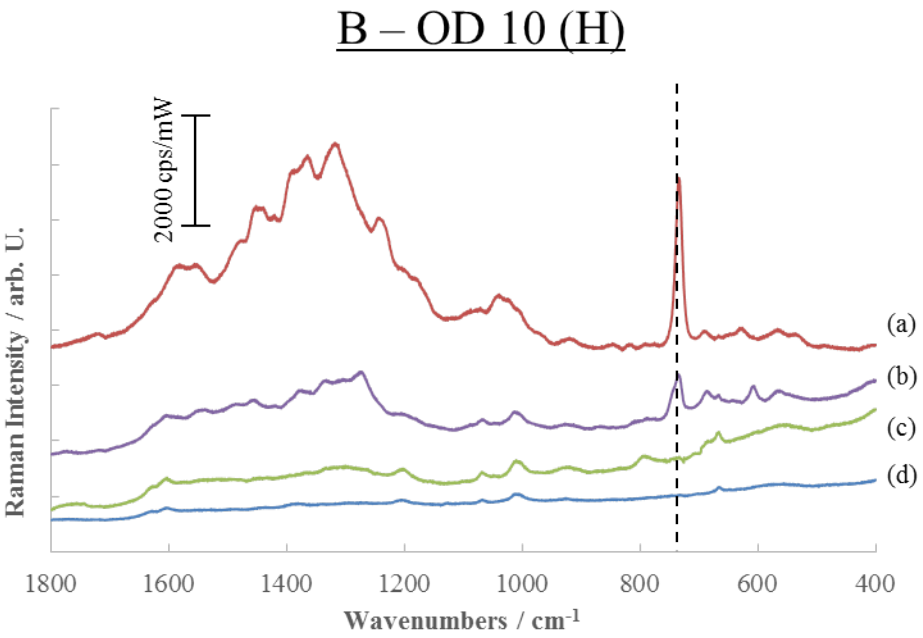
B – OD 10 (H)
2000 cps/mW
Raman Intensity / arb. U.
(a)
(b)
(c)
(d)
1800
1600
1400
1200
1000
800
600
400
Wavenumbers / cm-1

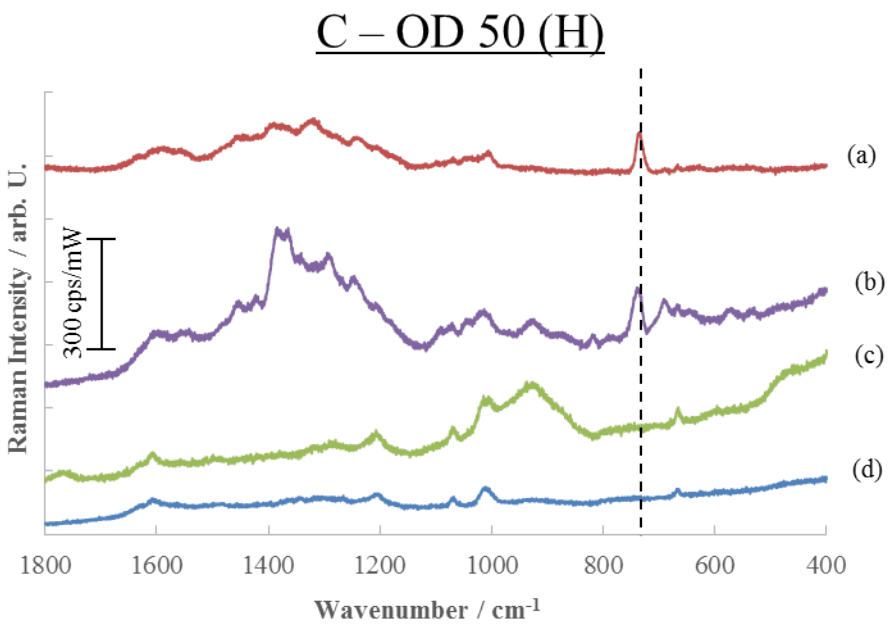
C – OD 50 (H)
Raman Intensity / arb. U.
300 cps/mW
(a)
(b)
(c)
(d)
1800
1600
1400
1200
1000
800
600
400
Wavenumber / cm-1

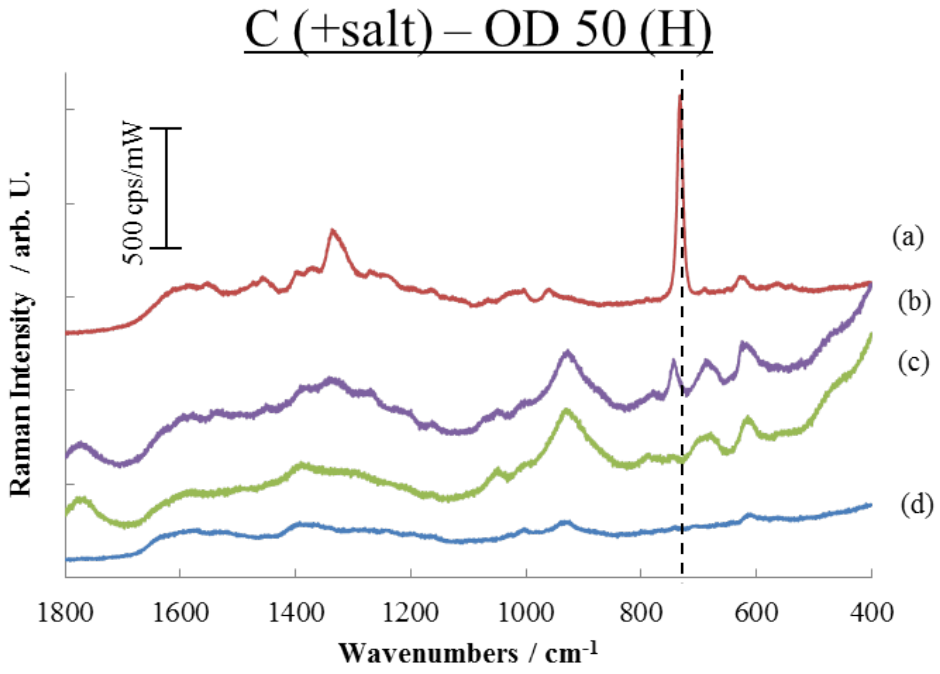
C (+salt) – OD 50 (H)
Raman Intensity / arb. U.
500 cps/mW
(a)
(b)
(c)
(d)
1800
1600
1400
1200
1000
800
600
400
Wavenumbers / cm-1